

N 739-65(18)

IITRI

IIT Research Institute

GPO PRICE \$
CSFTI PRICE(S) \$
Hard copy (HC)
Microfiche (MF)
ff 653 July 65

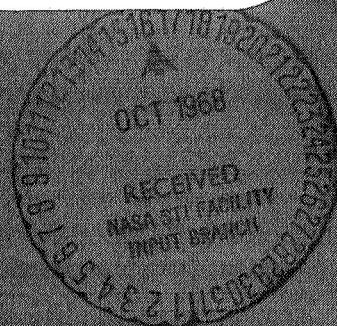
Report No. IITRI V6032-9
COMPOSITIONAL ANALYSIS OF LUNAR AND PLANET
SURFACES USING NEUTRON CAPTURE GAMMA RAY
to
Dr. V. R. Wilmarth
Code MAL
National Aeronautics and Space Administration
Washington, D. C. 20546

FACILITY FORM 602

N 68-36240

(ACCESSION NUMBER) 84
(PAGES) CR-97124
(NASA CR OR TMX OR AD NUMBER)

(THRU)
(CODE) 30
(CATEGORY)



Report No. IITRI V6032-9

COMPOSITIONAL ANALYSIS OF LUNAR AND PLANETARY
SURFACES USING NEUTRON CAPTURE GAMMA RAYS

to

Dr. V. R. Wilmarth

Code MAL

National Aeronautics and Space Administration
Washington, D. C. 20546

IIT RESEARCH INSTITUTE

Report No. IITRI V6032-9

COMPOSITIONAL ANALYSIS OF LUNAR AND PLANETARY
SURFACES USING NEUTRON CAPTURE GAMMA RAYS

July 1, 1967 to June 30, 1968

Prepared by

John H. Reed
and
John W. Mandler

Submitted by

IIT RESEARCH INSTITUTE
Technology Center
Chicago, Illinois 60616

to

Dr. V. R. Wilmarth
Code MAL
National Aeronautics and Space Administration
Washington, D. C. 20546

August 1968

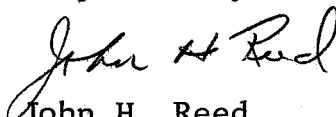
IIT RESEARCH INSTITUTE

FOREWORD

This is Report No. IITRI - V6032-9, an annual report under Contract No. NASr 65(18), entitled "Compositional Analysis of Lunar and Planetary Surfaces Using Neutron Capture Gamma Rays", covering the period July 1, 1967 to June 30, 1968.

The following personnel have contributed to the work described in this report; J. H. Reed, principal investigator, J. W. Mandler, co-investigator, R. A. Semmler, T. G. Stinchcomb, R. S. Ryskiewicz, and D. T. Krebs.

Respectfully submitted,



John H. Reed
Research Physicist
Group Leader
Nuclear & Radiation Physics

Approved:



Robert B. Moler
Manager
Nuclear & Radiation Physics

IIT RESEARCH INSTITUTE

ABSTRACT

COMPOSITIONAL ANALYSIS OF LUNAR AND PLANETARY SURFACES USING NEUTRON CAPTURE GAMMA RAYS

Capture gamma-ray and cyclic activation spectra from large granite and basalt models were obtained using a pulsed 14-MeV neutron source. Gamma rays from iron, silicon, oxygen, sodium, hydrogen (basalt only), aluminum (granite only), titanium (basalt only), and calcium (basalt only) were detected from these materials using a 3 in. x 3 in. NaI(Tl) detector. Inelastic neutron spectra were obtained with and without the use of a neutron reflector (which is used for the capture gamma-ray technique) to establish the compatibility of the inelastic and capture techniques. No interference was observed.

The development of computer codes to aid in the analysis of complex high energy gamma-ray spectra was initiated. GAUSS, a computer code developed by Heath et al., was modified to enable the code to determine the intensities (peak areas) of high energy gamma-ray lines. The modified program, GAUST, was tested on gamma-ray lines from 1.78 to 7.6 MeV and is currently being used to measure the intensity of gamma lines from iron, oxygen and hydrogen. Other programs, such as the Linear Least-Square Computer Program of Schmadebeck and Trombka, are currently being evaluated.

IIT RESEARCH INSTITUTE

A test of the capabilities of the combined neutron experiment is planned for the Fall of 1968. The probe (containing the 3 in. x 3 in. NaI(Tl) detector, the neutron generator and the appropriate neutron and gamma-ray shielding) that will be used during this test has been designed, fabricated, and tested.

A comprehensive study is currently being made to determine the advantages and disadvantages that a high resolution Ge(Li) detector would afford the combined neutron experiment. The preliminary spectra obtained with a 5 cm³ Ge(Li) detector indicate that such detectors promise to greatly increase the usable information obtainable from the combined neutron experiment.

TABLE OF CONTENTS

	<u>Page</u>
FOREWORD	ii
ABSTRACT	iii
LIST OF FIGURES	vii
I. INTRODUCTION	1
II. EXPERIMENTAL PROCEDURES	5
A. Experimental Apparatus	5
B. Neutron Monitoring	6
C. Timing	8
III. CORRECTION OF ELECTRONIC DEGRADATION OF THE SPECTRAL DATA	9
IV. EXPERIMENTAL RESULTS	13
A. Capture and Cyclic Activation Spectra From Basalt	13
B. Effect of Neutron Reflector	14
C. Detection of Hydrogen	16
D. Inelastic Spectrum From Basalt	17
E. Capture and Cyclic Activation Spectra From Granite	18
F. Spectrum From Basalt Obtained Using Ge(Li) Detector	19
V. COMPUTER ANALYSIS OF GAMMA-RAY SPECTRA	21
A. Peak Intensity and Position	21
B. Mathematical Smoothing of Gamma-Ray Spectra	26

IIT RESEARCH INSTITUTE

TABLE OF CONTENTS (Continued)

	<u>Page</u>
VI. DEVELOPMENT OF THE COMBINED-NEUTRON-EXPERIMENT DETECTOR PROBE	32
A. Selection of the Fast-Neutron Shadow Shield Material	32
B. Reflector Thickness	33
C. The Detector Shield Assembly	33
D. The Sandia Neutron Generator	34
E. General Probe Configuration	35
F. Weight of the Prototype Detector Probe	36
G. Data Acquisition Using the Probe	36
VII. SUMMARY	38
REFERENCES	41
APPENDIX: SAMPLES OF THE DIGITAL DATA OBTAINED DURING THE TEST OF THE COMBINED-NEUTRON-EXPERIMENT PROBE	

LIST OF FIGURES

Figure No.

- 2-1 VIEW OF THE EXPERIMENTAL CONFIGURATION
- 2-2 VIEW OF THE EXPERIMENTAL CONFIGURATION
- 2-3 VIEW OF THE ELECTRONICS
- 3-1 BLOCK DIAGRAM OF PREVIOUS DATA COLLECTING SYSTEM
- 3-2 OSCILLOSCOPE TRACES OF EFFECTS OF BIPOLAR PULSE ON ND-130 PULSE HEIGHT ANALYZER
- 3-3 OSCILLOSCOPE TRACES OF EFFECTS OF UNIPOLAR PULSE ON ND-130 PULSE HEIGHT ANALYZER
- 3-4 BLOCK DIAGRAM OF CURRENT DATA COLLECTING SYSTEM
- 3-5 GRANITE-CAPTURE SPECTRUM (Short Delay - High Output)
- 4-1 BASALT-CAPTURE AND CYCLIC ACTIVATION SPECTRA (High Energy)
- 4-2 BASALT-CAPTURE AND CYCLIC ACTIVATION SPECTRA (Low Energy)
- 4-3 BASALT-CAPTURE GAMMA-RAY SPECTRUM (Background Subtracted, High Energy)
- 4-4 BASALT-CAPTURE GAMMA-RAY SPECTRUM (Background Subtracted, Low Energy)
- 4-5 BASALT-CAPTURE AND CYCLIC ACTIVATION SPECTRA (4 cm Polyethylene)
- 4-6 BASALT-CAPTURE AND CYCLIC ACTIVATION SPECTRA (No Reflector)
- 4-7 BASALT-CAPTURE AND CYCLIC ACTIVATION SPECTRA (4 cm Polyethylene with lead shield)
- 4-8 BASALT-INELASTIC SPECTRUM (No Reflector)

IIT RESEARCH INSTITUTE

LIST OF FIGURES (Continued)

Figure No.

- 4-9 BASALT-INELASTIC SPECTRUM (8-cm Polyethylene)
- 4-10 GRANITE-CAPTURE SPECTRUM (8-cm Paraffin)
- 4-11 GRANITE-CYCLIC ACTIVATION SPECTRUM
(8-cm Paraffin)
- 4-12 COMPARISON OF BASALT AND GRANITE
- 4-13 BASALT-CAPTURE SPECTRUM (5-cm³ Ge(Li)
Detector)
- 4-14 VIEW OF EXPERIMENTAL CONFIGURATION USING
Ge(Li) DETECTOR
- 5-1 COMPARISON OF SMOOTHED AND UNSMOOTHED
SPECTRUM
- 6-1 VIEW OF SANDIA GENERATOR TYPE 26C
- 6-2 VIEW OF THE COMBINED-NEUTRON-EXPERIMENT
DETECTOR PROBE (No Reflector)
- 6-3 VIEW OF THE COMBINED-NEUTRON-EXPERIMENT
DETECTOR PROBE (8-cm Polyethylene)
- 6-4 BASALT-CAPTURE AND CYCLIC ACTIVATION
SPECTRA (Using Probe and 8-cm Polyethylene)
- 6-5 BASALT-INELASTIC SPECTRUM (Using Probe and
8-cm Polyethylene)

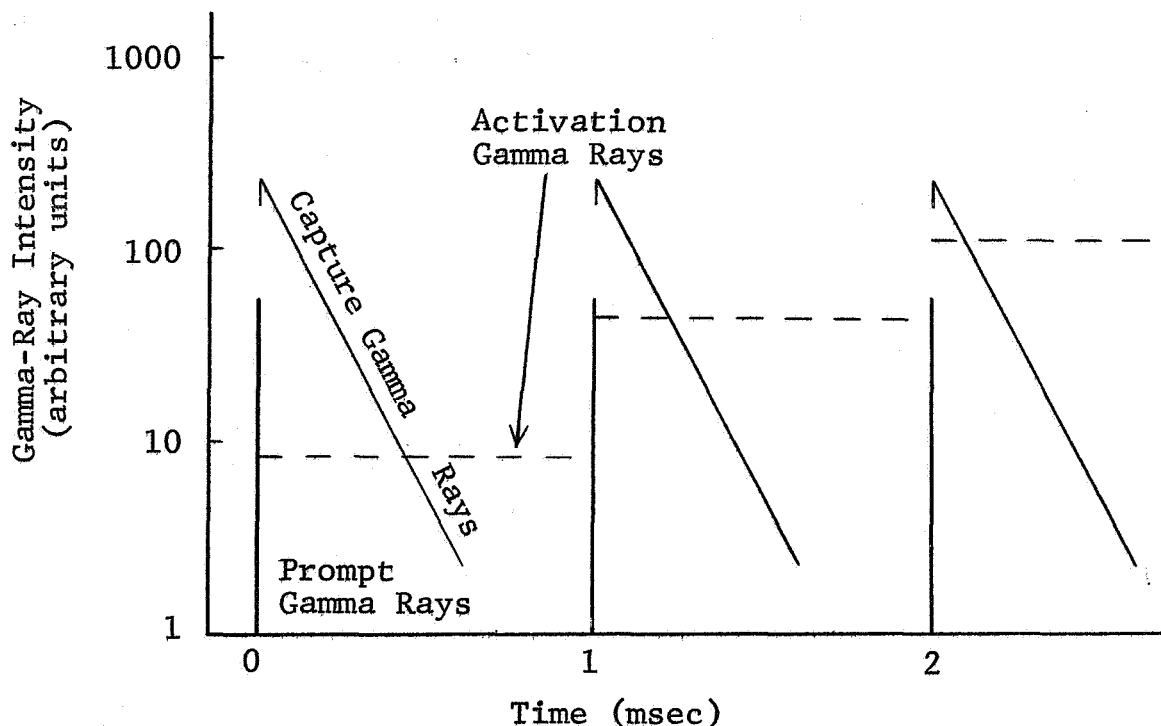
I. INTRODUCTION

One of the objectives of the space program is to ascertain the composition of lunar and planetary surfaces. This information is of great importance to those in the scientific community who are concerned with the origin and the evolution of the moon and planets. Since it does not appear that a significant number of samples will be available from the planets, remote analysis of these surfaces is required. A technique for remote elemental analysis, alpha-scattering, has been developed and was successfully used on several of the Surveyor spacecraft.^(1,2) However, this technique is sensitive to a layer extending only a few microns below the surface and it cannot identify specific elements with masses above approximately 40. For these reasons NASA is presently developing a combined neutron experiment⁽³⁾ which has the capabilities of performing compositional analysis on a layer extending 10 to 15 cm below the surface without any mass restrictions.

This combined experiment will utilize four different neutron analytical methods (capture gamma-ray analysis, fast-activation analysis, inelastic neutron scattering, and thermal neutron die-away). The four techniques are being integrated into a single package and will use the same gamma-ray detector, 14-MeV neutron source, and multichannel pulse height analyzer. Elemental compositions can be determined by three of the methods

(capture gamma-ray analysis, activation analysis, and inelastic neutron scattering); the presence of hydrogen can be determined by two of the methods (capture gamma-ray analysis and neutron die-away); and density information will be provided by the neutron die-away technique. Therefore, the combined neutron experiment will provide elemental information with the desired redundancy to provide cross-checks.

The sketch below shows the time relationship of the gamma rays present in the combined neutron experiment. Inelastic gamma rays are present only during the neutron pulse while the intensity of the capture gamma rays builds up during the pulse and dies away after the pulse. The activation gamma-ray intensity builds up during each pulse and exhibits negligible decay between pulses since the half-lives are long compared to the time between pulses.



TIME RELATIONSHIP OF THE GAMMA RAYS
PRESENT IN THE COMBINED NEUTRON EXPERIMENT

IIT Research Institute has been assigned the responsibility of developing the capture gamma-ray portion of the combined experiment, and this report is primarily concerned with the present status of the capture gamma-ray experiment which includes collection and analysis of the capture gamma-ray spectra.

During the first year of the research effort (May 1, 1966 to June 30, 1967) the feasibility of using the capture gamma-ray and cyclic activation techniques with a pulsed source of high-energy neutrons and a semi-infinite sample was demonstrated. Pure sand and iron-sand samples were used for these studies. The necessary electronics for gating of the pulse height analyzer (PHA) and for routing of the data obtained during the two sampling periods into different halves of the PHA memory were designed and constructed. During these initial studies it was found that the intensity of the capture gamma rays could be greatly enhanced by placing a hydrogenous reflector material above the neutron source, thereby utilizing some of the neutrons normally lost to the atmosphere.

During the present reporting period the iron-sand sample was replaced by homogeneous samples of crushed granite and basalt. Several problems encountered during the first year were solved and a more optimum neutron output was used, allowing sampling to begin as soon as 10 μ sec after the neutron burst. A lead shield was placed between the reflector and the detector in order to shield the detector from hydrogen capture gamma rays produced in the reflector. With this shield the detection of hydrogen

IIT RESEARCH INSTITUTE

can be accomplished without forfeiting the benefits of a neutron reflector.

A Sandia generator was obtained during this reporting period and it was successfully used to obtain capture, cyclic activation, and inelastic gamma-ray spectra from basalt. A prototype probe was designed, constructed, and used with the Sandia generator to obtain gamma-ray spectra from basalt. Finally, computer programs for spectral analysis were evaluated and investigations were begun to modify existing programs for our use.

II. EXPERIMENTAL PROCEDURES

The ultimate objective of the combined neutron experiment has dictated the use of very large samples and a 14-MeV neutron source for the development studies. A description of the experimental apparatus and procedures that have been used for the capture gamma-ray portion of the experiment follows.

A. Experimental Apparatus

The gathering of the necessary capture and cyclic activation gamma-ray spectra requires the use of large samples. A 60- x 60- x 30-in. plywood box filled with a crushed sample provided a very convenient approximation to a semi-infinite medium. Samples of granite and basalt were used. The granite is No. 1 mesh, Burnet Red Granite, and was obtained from the Bilbrough Marble Co., Burnet, Texas. Its measured bulk density is 1.50 gm/cm^3 . The basalt is 1/4 in.-to-20-mesh Knippa-type basalt and was obtained from Trinity Concrete Products, Dallas, Texas. Its measured bulk density is 1.82 gm/cm^3 . Both the granite and basalt are the same type used by Mills and Givens⁽⁴⁾ for their neutron die-away experiments.

The detection of the gamma rays was accomplished using a 3 in. x 3 in. NaI(Tl) crystal optically coupled to a RCA 8054 photomultiplier (PM) tube. A thermal neutron shield consisting of Li^6F ($47 \text{ gm/cm}^2 \text{ Li}^6$) surrounded the crystal. Shielding of the crystal from fast neutrons was accomplished by placing a

IIT RESEARCH INSTITUTE

6-in.-long shadow shield between the neutron source and the crystal. Several shadow shield materials (copper, tungsten, and molybdenum) and shapes (cylindrical and truncated cones) were used. Various thicknesses of neutron reflector material (polyethylene or paraffin) were placed above the neutron source in order to increase the thermal flux on the surface of the sample. The electronics used for data collection are discussed in Section III.

Figures 2-1, 2-2, and 2-3 are photographs of the experimental setup showing the crystal, shadow shield, neutron reflector, Van de Graaff, and electronics.

B. Neutron Monitoring

The IITRI Van de Graaff generator was used in the pulsed mode to produce the 14-MeV neutrons for the capture gamma-ray experiments via the $H^3(H^2, n)He^4$ reaction. Previously⁽⁵⁾ the 14-MeV neutron output of the Van de Graaff generator was monitored by a BF_3 counter positioned under the large sample container. Neutron output measurements were performed using copper activation foils to obtain the 14-MeV neutron output per BF_3 count, enabling a BF_3 count rate to be related directly to 14-MeV neutron output. This method of monitoring the 14-MeV neutron output had the disadvantages that, for a given 14-MeV neutron output, the BF_3 count rate was sensitive to the sample material and to the

amount of reflector material used.

Because of these disadvantages, a neutron monitoring system employing a plastic scintillator and a Teflon sample* placed near the target (neutron source) was devised. The plastic scintillator output is directed through a discriminator which is adjusted (using a Pu-Be neutron source) to pass only counts from neutrons whose energies are greater than about 9 MeV. The F^{18} activity in the Teflon produced by the $F^{19}(n,2n)F^{18}$ reaction ($Q = -10.4$ MeV) is gross-counted using a NaI(Tl) well-crystal. Both the plastic scintillator and the Teflon are calibrated using copper activation foils so that a scintillator count rate can be related directly to 14-MeV neutron output. Since these two methods are sensitive only to high-energy neutrons, they are independent of sample material and reflector thickness.

The plastic scintillator is also used during the setup of the capture gamma-ray runs to monitor the neutrons produced between pulses. This is done to ensure that the neutron generator is pulsing correctly and not producing appreciable dark current (neutrons between pulses). Using the plastic scintillator, it is found that the dark current from the Van de Graaff is negligible for a 40- μ sec pulse width but frequently is high for a 10 μ sec pulse width. Although the generator which will be used in the combined experiment uses about a

* Suggested by W. R. Mills, Mobil Oil Corporation.

10- μ sec pulse width (the Sandia generator exhibits negligible dark current when operated at a 10- μ sec pulse width), the Van de Graaf was operated primarily with a 40- μ sec pulse width.

C. Timing

To obtain the capture and cyclic activation gamma-ray spectra, the Van de Graaff was operated at a pulse rate of about 500 per second. As mentioned above, the pulse duration was 40- μ sec. The combination capture gamma-ray and cyclic activation spectrum was obtained by sampling during the period 20 - 254 μ sec after each neutron pulse while the cyclic activation spectrum was obtained by sampling during the period 1370 - 1604 μ sec after each pulse (i.e., just before each pulse). The electronics used to accomplish this sampling are described in Section III. of this report and in Reference 5.

III. CORRECTION OF ELECTRONIC DEGRADATION OF THE SPECTRAL DATA

Degradation of the gamma-ray spectrum had been evident under the following two conditions:⁽⁶⁾ 1) if the sampling was begun within 100 μ sec after the end of the neutron burst, and 2) if the neutron output was greater than approximately 7000 neutrons per pulse. This degradation consisted of a general deterioration of energy resolution as well as such an unusually large number of counts in the low-energy region of the spectrum that gamma lines below about 1 MeV were completely obscured.

These spectrum-degradation problems were traced to the manner in which the ND 130 multichannel analyzer was used. In review, the slow, low-level pulses from the preamplifier were amplified and shaped by a Tennelec TC 200 amplifier. The resulting 0-to 10-V bipolar pulses were applied to the pulse height analyzer. In addition, a signal from the analyzer sequence switch was applied to the coincidence input of the analyzer to activate the analyzer at the desired times after each neutron burst (see Figure 3-1). Since the pulses entering the analyzer appeared to be normal, undistorted, bipolar pulses, the analyzer itself became suspect and the pulse-handling capacity of the ND 130 was studied in detail. The results of this study are outlined by the series of oscilloscope traces presented in Figures 3-2 and 3-3.

If a 10-V bipolar pulse is presented to the analyzer,

IIT RESEARCH INSTITUTE

the input circuitry clips the negative portion off (by using of a diode), attenuates, and inverts the pulse. A negative pulse of 1.7-V amplitude results at the input of the analog to digital converter (ADC). Associated with this pulse, however, is a positive overshoot followed by a negative overshoot. The negative overshoot has a very long time constant (see Figure 3-2d). After a delay of 30 μ sec, the amplitude of this overshoot is still 0.1 V (which corresponds to a gamma equivalent of 600 keV, if a 10-V input pulse at the analyzer corresponds to a 10-MeV gamma ray, as is typical), and becomes negligible only after about 100 μ sec. This characteristic of the ND 130 is indeed troublesome because the presence of this overshoot at the time of application of an enable level to the coincidence input is immediately interpreted as a gamma pulse of the corresponding magnitude and is therefore analyzed and stored. Also, if a gamma-ray pulse is superimposed on this overshoot at the time of application of an enable level, the sum of the gamma-ray pulse and the overshoot is analyzed and stored. This yields spurious high-energy counts and reduced energy resolution. For these reasons, sampling sooner than 100 μ sec after the end of a neutron burst results in spectral distortion (high low-energy count rate and reduced energy resolution).

If the input signal is unipolar rather than bipolar, this negative overshoot is eliminated (see Figure 3-3a and b). Therefore, for applications such as the capture gamma-ray experiment, it is mandatory that the input pulse to the analyzer be unipolar.

IIT RESEARCH INSTITUTE

The manual for the ND 130 warns that, in coincidence operation in those situations where an enable level arrives at the coincidence input but no detector signal occurs, a memory cycle will normally be produced by the transient generated by the closing of the linear gate. Thus, a memory cycle is initiated for each sampling period (two for each neutron pulse) whether or not a signal pulse is present.

As a result of the above investigation, a new pulse-handling system was devised (see Figure 3-4) and is presently being used. A unipolar pulse is used at the input of the ND 130 and an external linear gate is used to select the pulses reaching the analyzer. This system has the desired properties: 1) the long-term overshoot in the ADC is eliminated by the use of the unipolar pulse at the input of the ND 130; 2) the internal coincidence circuit is not used; and 3) bipolar pulses can be and are used prior to the biased amplifier where the pulse count rates may be high.

This new pulse system has been used with and without the low-level discriminator (LLD) indicated in Figure 3-4. If the linear gate is strobed by the LLD while the enable level from the analyzer sequence switch is present, the signal is allowed to enter the ND 130. Without the action of the LLD the possibility exists that the linear gate will open while the "tail" of a preceding pulse is present. Experimentally, we have observed no discernible difference between spectra obtained with and without the LLD requirement. Apparently the count

IIT RESEARCH INSTITUTE

rates involved are sufficiently low that the probability of a "tail" being present when the linear gate opens is small.

Figure 3-5 shows a capture gamma-ray spectrum of granite obtained using the system described above and the geometry described in Reference 5. This spectrum was obtained with a short delay (50 μ sec after the neutron pulse) and with high-neutron output per pulse (11,140 neutrons/pulse). The gamma rays in the region below 1 MeV are no longer masked, the energy resolution of the spectrometer is normal, and the extraneous high-energy peaks are eliminated. It is believed that the spectrum degradation problems have been solved.

IV. EXPERIMENTAL RESULTS

Capture, inelastic, and cyclic activation gamma-ray spectra were obtained from large basalt and granite samples. The samples and the methods used to obtain the spectra were discussed in Section II. The capture and cyclic activation spectra were obtained using several reflector thicknesses in order to ascertain the advantage of each thickness. The inelastic spectrum from basalt was obtained with and without the presence of the reflector to establish the compatability of the inelastic and capture experiments.

A. Capture and Cyclic Activation Spectra from Basalt

Figure 4-1 shows the high-energy capture and cyclic activation gamma-ray spectra from basalt obtained using an 8-cm-thick paraffin reflector located above the neutron source. The pulse rate was 493 pulses per second, the pulse duration was 10 μ sec, and the output was 3420 neutrons per pulse. Although, as noted in Section II, the dark current was frequently high when the pulse width was 10 μ sec, the dark current was not excessibe for any of the spectra shown in this section, regardless of the pulse width used. Capture gamma rays from iron, titantium, calcium, silicon, sodium, and hydrogen have been identified in curve A (combined capture plus activation spectrum) of Figure 4-1. Most of the hydrogen capture gamma rays present in this

spectrum originated in the paraffin reflector. Curve B (cyclic activation spectrum) shows the presence of silicon and oxygen.

The low-energy capture and cyclic activation gamma-ray spectra from basalt is shown in Figure 4-2. These spectra, obtained under the same conditions as those of Figure 4-1, show the presence of iron, titanium, calcium, silicon, and hydrogen. Again the hydrogen capture gamma rays are from the paraffin reflector.

To obtain the pure capture gamma-ray spectra, each cyclic activation spectrum was subtracted from the corresponding combined capture plus activation spectrum (i.e., curve B was subtracted from curve A in Figures 4-1 and 4-2). The results of these subtractions are shown in Figures 4-3 and 4-4. In the low-energy region the subtraction results in the enhancement of the 1.91-MeV line from calcium and the 1.39-MeV titanium line through the removal of the silicon activation lines and the natural background. The oxygen activation lines are removed from the high-energy spectrum thereby enhancing the silicon and calcium lines.

B. Effect of Neutron Reflector

The spectra shown in Figures 4-1 through 4-4 were obtained using an 8-cm-thick reflector located above the neutron source. The purpose of this reflector is to utilize a portion of the 14-MeV neutrons normally lost to the atmosphere by reflecting them back toward the sample. Since these reflected neutrons are of

IIT RESEARCH INSTITUTE

lower energy, the thermal neutron flux on the surface of the sample is increased.

In order to determine the effects of different reflector thicknesses, capture and cyclic activation gamma-ray spectra were obtained from basalt using three reflector thickness (0 cm, 4 cm, and 8 cm). The other conditions under which the spectra were obtained were identical. In each case the area under the 7.6-MeV iron peak in the capture gamma-ray spectrum was obtained together with the area under the 6.1-MeV oxygen peak in the cyclic activation spectrum. The computer program GAUST, which is discussed in Section V, was used to obtain these areas. Table 4-1 shows the results of the measurements. Examination of these results indicates that a 4-cm-thick reflector increases the intensity of the capture gamma rays by about 75 percent and an 8-cm-thick reflector increases their intensities by about a factor of 2.5. Neither reflector affected the 14-MeV flux on the surface of the sample, as evidenced by the constant area under the oxygen peak for the different reflectors.

Table 4-1
EFFECT OF REFLECTOR THICKNESS

Reflector Thickness (cm)	Area Under Iron Peak (counts)	Area Under Oxygen Peak (counts)
0	605 \pm 118	1098 \pm 76
4	1077 \pm 107	968 \pm 87
8	1628 \pm 226	1023 \pm 72

C. Detection of Hydrogen

As indicated in the discussion of Figure 4-1, the use of a hydrogenous reflector causes an intense hydrogen capture gamma-ray peak in the spectrum, therefore detection of hydrogen in the sample was impossible. Since the detection of hydrogen is of prime concern to the capture gamma-ray experiment and the use of a neutron reflector is beneficial to the experiment, a study was made to determine how the detection of hydrogen could be accomplished using capture gamma rays without forfeiting the use of a neutron reflector.

Figure 4-5 shows the capture and activation spectra from basalt obtained using a 4-cm-thick polyethylene reflector located above the neutron source. Figure 4-6 shows the capture and activation spectra from basalt obtained under the same conditions as those of Figure 4-5 with the exception that no reflector was used. In Figure 4-6 the 2.22-MeV hydrogen capture gamma-ray peak is due solely to hydrogen in the basalt sample, while in Figure 4-5 it is due to both the sample and the reflector. A comparison (after normalization to a common thermal neutron flux by means of the number of counts in the 7.6-MeV iron capture gamma-ray peaks) of the areas of the two hydrogen peaks indicates that 44 ± 13 percent of the counts in the hydrogen peak in the spectrum obtained using a 4 cm reflector is due to the reflector with the remainder coming from the basalt sample.

Figure 4-7 shows the spectrum from basalt obtained under the same conditions as for Figure 4-5 with the exception that a 4-in.-thick lead shield was located between the crystal and the polyethylene neutron reflector. The purpose of the lead shield was to prevent hydrogen capture gamma rays originating in the reflector from reaching the crystal (4-in. of lead attenuates the 2.22-MeV hydrogen capture gamma rays by about a factor of 200). A comparison (after normalization to a common thermal flux) of the spectra obtained with and without the lead shield indicates that to within statistical error (2028 ± 475 counts for Figure 4-7 vs. 2703 ± 475 for Figure 4-6) the number of counts in the hydrogen capture gamma-ray peaks in both figures are the same.

The results of the above measurements indicate that the detection of hydrogen can be accomplished using capture gamma rays without forfeiting the use of a neutron reflector if the crystal is shielded from the gamma rays produced in the reflector. Aside from the beneficial effect of eliminating the counts due to gamma rays produced in the reflector, this shield appears to have no effect on the capture gamma-ray spectrum.

D. Inelastic Spectrum from Basalt

In order to determine what effect the neutron reflector has on the inelastic spectrum from basalt, inelastic spectra were obtained both with an 8-cm-thick polyethylene reflector

and without any reflector. To obtain these spectra the Van de Graaff was operated at 8870 pulses per second with a 10- μ sec pulse duration. Figure 4-8 shows the inelastic spectrum obtained from basalt using an output of 84 ± 9 neutrons per pulse and no reflector. Figure 4-9 shows the corresponding spectrum obtained using an output of 65 ± 12 neutrons per pulse and an 8-cm-thick polyethylene reflector.

A comparison of these spectra indicates that the reflector does not affect the spectral shape of the inelastic spectrum. A comparison (after normalization to a common 14-MeV output) of the intensities of the 6.1-MeV oxygen peaks in the two spectra shows that, within statistics, the intensities are the same (522 ± 82 counts using the reflector vs. 650 ± 133 using no reflector). The above results indicate that the use of a neutron reflector affects neither the shape nor the intensity of the inelastic spectrum.

E. Capture and Cyclic Activation Spectra from Granite

Figure 4-10 shows the combination capture plus activation spectrum from granite. To obtain this spectrum an 8-cm-thick paraffin reflector was located above the neutron source. The pulse rate was 493 pulses per second, the pulse duration was 10 μ sec, and the neutron output was 2490 neutrons per pulse. Capture gamma-ray peaks from iron, aluminum, sodium, silicon,

and hydrogen have been identified in this spectrum. Again, most of the hydrogen capture gamma rays are from the reflector.

The cyclic activation spectrum from granite is shown in Figure 4-11. This spectrum was obtained concurrently with Figure 4-10 so that the conditions under which it was obtained are identical to those for Figure 4-10. Cyclic activation peaks from oxygen and silicon are present in this spectrum together with background peaks from potassium-40, natural thorium, and the uranium-238 chain.

A comparison of the combined capture plus activation spectra from granite and basalt is shown in Figure 4-12. The two spectra were taken under similar conditions, the only difference being in the neutron outputs used. It is evident that these spectra are markedly different - the capture gamma rays dominate the basalt spectrum, while activation gamma rays from oxygen and silicon and background gamma rays are the dominant features of the granite spectrum.

F. Spectrum From Basalt Obtained Using Ge(Li) Detector

The combined capture plus cyclic activation spectrum from basalt was obtained using a 5-cm³ Ge(Li) detector. This spectrum, shown in Figure 4-13, was obtained using a pulse rate of 760 per second and a 40-μsec pulse duration, and an output of $4.3 (\pm 0.5) \times 10^4$ neutrons per pulse. A 4-cm-thick polyethylene neutron reflector was located above the neutron

source, and the gamma rays from the reflector were shielded from the detector by a 4-in. lead shield (see Figure 4-14).

Comparison of this spectrum with the corresponding spectrum obtained using a NaI(Tl) detector (Figure 4-5) shows the effect of using a higher resolution detector. Many of the peaks which were unresolved in the NaI(Tl) spectrum appear as single peaks in the Ge(Li) spectrum. Hydrogen, which was detected in the NaI(Tl) spectrum, is not present in the Ge(Li) spectrum, probably because the detection efficiency of the 5 cm³ detector is about at its minimum for this energy region. However, manganese-56 is observed in the Ge(Li) spectrum while it does not seem to be present in the NaI(Tl) spectrum. The quality of the spectrym in Figure 4-13 is not optimum since the detector was quite small and the neutron output was not optimized for this type of detector.

V. COMPUTER ANALYSIS OF GAMMA-RAY SPECTRA

Neutron capture, inelastic scatter, and, to lesser degree, cyclic activation produce complex gamma-ray spectra. Each spectrum contains peaks that are characteristic of the material being inspected. It is the purpose of an analysis scheme to determine the source (the element) and intensity (relative abundance) of the gamma-ray lines which cause these peaks. If we assume the efficiency of the detector is known, the quantity of interest is the number of pulses recorded from full-energy interactions caused by a particular gamma-ray.

A. Peak Intensity and Position

To determine the intensity of a given peak from the pulse height spectrum is generally not a simple problem. The peak must be located and identified, the background must be precisely taken into account, and the statistical fluctuations must be rigorously considered. A literature search was conducted to find existing computer programs for the analysis of complex gamma-ray spectra which are directly applicable to our data or which could be modified for use at our computer facility.

Of the several methods we have studied, the one which seems most suitable for the analysis of spectra from this experimental program is the method developed by Trombka and his associates.⁽⁷⁾ This method uses a library of standard pulse height spectra with source energies from zero to the equivalent

of maximum pulse height in increments which are small compared to the peak width (as determined by the resolution of the detector). It locates peak positions (to an accuracy determined by the magnitude at the increments) and determines peak intensities. The library of standard spectra up to source energies of 3 MeV is now available from Goddard Space Flight Center, but the standard spectra from 3 MeV to 8 MeV (which are needed for the data analysis of this experimental program) will not be available for some time.

Until the complete library becomes available and the method is thoroughly tested, a less suitable method of data analysis will have to be used. Consequently, two programs (PIKPEEK and GAUSS) have been adapted for our use. Program PIKPEEK⁽⁸⁾ scans gamma-ray spectral data and locates the peaks if the resolution function of the spectrometer is specified. PIKPEEK has been applied to capture gamma-ray spectra and it successfully located most, if not all, the peaks and shoulders that could be located visually. This code is not being used at present, but may be of future use when data are being analysed by computer on a routine basis.

Program GAUSS⁽⁹⁾ determines peak intensities and precise locations if an initial estimate of the peak position is known. GAUSS assumes that the region being analyzed is composed of a Gaussian shaped peak plus a linear background. We have modified GAUSS for use with our data. This modification consists of several extensions which are described in the following paragraphs.

III RESEARCH INSTITUTE

The first modification simply provided for a description of the background by using a quadratic function instead of a linear function. GAUSS was originally programmed for the analysis of large peaks of low-energy gamma lines superimposed on a relatively small background. A linear approximation to the background was adequate. Our application requires the analysis of small peaks of high-energy gammas superimposed on a relatively large background. Consequently, a better approximation of the background is necessary.

The initial attempt at using a quadratic background did not provide a good fit to the data on the lower energy side of the peak for high energy peaks (6 to 7 MeV). One cause of the lack of fit is the Compton edge which is present with full-energy peaks at these high energies. An additional parameter was included which takes into account this Compton edge. It was also noted that the high-energy tail of the first escape peak at these energies perturbs the shape of the full-energy peak. Therefore, an additional parameter was included to account for the effects of the first escape peak.

The two parameters mentioned in the previous paragraph were included in the program by substituting them for the parameters α_1 and α_2 which were used in the original program to account for small departures of the peak from a true Gaussian shape. These departures are negligible compared to statistical fluctuations unless the peak is quite large.

Mathematically, the modifications discussed so far can be described as a change in the function representing the number of counts y_i in channel x_i from

$$y_i = ax_i + b + \sum_j h_j \exp \left[-4 \ln 2 \cdot \left(\frac{x_i - x_j}{w_j} \right)^2 \right] \cdot \left[1 + \alpha_{1j} (x_i - x_j)^{m_1} + \alpha_{2j} (x_i - x_j)^{m_2} \right] \quad (1)$$

to

$$y_i = ax_i + b + cx_i^2 + \sum_j h_j \left\{ \exp \left[-4 \ln 2 \cdot \left(\frac{x_i - x_j}{w_j} \right)^2 \right] + g_j \exp \left[-4 \ln 2 \cdot \left(\frac{x_i - x_j + x_e}{w_j} \right)^2 \right] + f_j \int_{x_i}^{\infty} \exp \left[-4 \ln 2 \cdot \left(\frac{z - x_j + x_c}{w_j} \right)^2 \right] \frac{2}{w_j} \frac{dz}{\sqrt{\frac{\ln 2}{\pi}}} \right\} \quad (2)$$

The summation is over the number of peaks. The program can accept 10 peaks with the limitation that the number of parameters to be fitted should not exceed 50. Our experience, however, has been limited to the analysis of one peak at a time. The parameters to be fitted are the background parameters a , b , and c plus five parameters for each peak:

h_j , the peak height
 x_j , the peak center
 w_j , the peak width (FWHM)
 g_j , the escape peak parameter
 f_j , the Compton edge parameter.

The quantities x_e and x_c are the displacements of the escape peak and Compton edge, respectively, from the full-energy peak. These are input quantities replacing m_1 and m_2 .

The modifications gave a much better fit to the data on the low-energy side of the full-escape peak and resulted in a lowered value for chi-squared, which is a measure of the goodness-of-fit.

To provide for initial values of the background parameters and of the heights of the full-energy peaks (which are necessary input to GAUSS), the program was modified to incorporate a linear least squares computation of these initial values. An accompanying revision in the program allows one to select whether these initial values shall be given as input data or be calculated by the program. The revision also allows the initial values of g_j and f_j to be calculated in the same manner as the initial value of w_j in the original version.

These revisions have resulted in a data-analysis program (designated GAUST) which has been satisfactory for the analysis of peaks from iron (7.6 MeV), oxygen (6.1 MeV), hydrogen (2.2 MeV), and silicon (1.8 MeV).

B. Mathematical Smoothing of Gamma-Ray Spectra

Often, experimental data are used to determine the parameters which describe a physical situation. Examples of these are the area of a peak in a gamma-ray spectrum and the description of the background upon which the peak is superimposed.

A technique that could successfully remove the statistical scatter from observed gamma-ray spectra would be of considerable aid in data interpretation. One type of data convolution⁽¹⁰⁻¹³⁾ that has been widely used for many years has been studied to determine its benefits and its limitations. This method computes a new value of each datum in the spectrum based on a least-squares fit of a polynomial to a small region of the raw data. (Details of the method have been described by Savitzky and Golay.⁽¹²⁾). The resulting data points are known as the convoluted or smoothed data. The statistical error in each datum point can be reduced appreciably by this technique, and the spectra do appear superior as demonstrated by the two curves in Figures 5-1. The points in curve A are the original data points and the curve drawn through these points represents visual smoothing of these data points. Curve B shows the data points after mathematical smoothing was performed on the original data.

Least-square fitting programs (e.g., GAUST) are often used to calculate various parameters of a spectrum (e.g., area under a peak). The question then arises, "Can the accuracy of an estimated value of a parameter be improved by using the

smoothed data instead of the experimental data, and if so, how great is the improvement?" The following discussion is addressed to this question.

Assume that the following relationship describes a physical situation

$$y = \sum_{m=1}^M a_{om} f_m(x), \quad (3)$$

where the M values of the parameters a_{om} are unknown and are to be determined by I measurements of y at different values of x using equal spacing. Thus $x_i = x_1 + (i-1)\Delta x$. Denote the corresponding true values of y by y_{oi} and the measured values by y_i . The probability that one of the measured values falls between y_i and $y_i + dy$ is

$$P(y_i)dy_i = \exp \left[-(y_i - y_{oi})^2 / 2\sigma_{yi}^2 \right] dy_i / (\sqrt{2\pi} \sigma_{yi}) \quad (4)$$

Using a least-squares fit to the measured values of the y_i , a set of estimated a_m of the parameters a_{om} is obtained:

$$\sum_{i=1}^I \left[y_i - \sum_m a_m f_m(x_i) \right]^2 / \sigma_{yi}^2 = \text{minimum}. \quad (5)$$

The weights, $1/\sigma_{yi}^2$, may be denoted by w_i for convenience. The minimum condition leads to

$$\sum_i \left[y_i - \sum_m a_m f_m(x_i) \right] w_i f_\ell(x_i) = 0. \quad (6)$$

IIT RESEARCH INSTITUTE

For simplicity, let us assume that these weights are nearly the same for all the I channels and can (to a first approximation) be considered equal. Then letting

$$F_{\ell m} = \sum_{i=1}^I f_{\ell}(x_i) f_m(x_i), \quad (7)$$

one has

$$a_m = \sum_{k=1}^M F_{mk}^{-1} \sum_{i=1}^I \left[f_k(x_i) y_i \right], \quad (8)$$

where the $F_{m\ell}^{-1}$ are the elements of the matrix resulting from the inversion of the symmetric matrix defined by Equation 7.

Since the y_i are statistically independent, the square of the deviation in the estimated a_m is given by

$$\sigma_{a_m}^2 = \sum_{\ell} \sum_k F_{\ell m}^{-1} F_{km}^{-1} \sum_i \left[f_{\ell}(x_i) f_k(x_i) \sigma_{yi}^2 \right]. \quad (9)$$

Since the weights are considered equal, σ_y^2 is independent of i , and one obtains

$$\sigma_{a_m}^2 = \sigma_y^2 F_{mm}^{-1}. \quad (10)$$

Now suppose that the data are smoothed before applying the least-squares fit. Consider a smoothing over $2q + 1$ channels with normalized weights p_0, p_1, \dots, p_q such that

$$p_0 + 2(p_1 + p_2 + \dots + p_q) = 1 \quad . \quad (11)$$

Another set of estimates of the parameters a_{om} can then be obtained. This set can be denoted by a_{sm} . The smoothed data points, y_{si} , are given by

$$y_{si} = p_0 y_i + \sum_{j=1}^q p_j (y_{i-j} + y_{i+j}) \quad , \quad (12)$$

and a_{sm} is therefore given by

$$a_{sm} = \sum_k F_{mk}^{-1} \sum_i \left[f(x_i) y_{si} \right] \quad . \quad (13)$$

Since the y_{si} are not statistically independent, the square of the deviation of a smoothed parameter cannot be written using a formula similar to Equation 9. However, Equation 13 can be written in terms of the y_i which are statistically independent:

$$a_{sm} = \sum_k F_{mk}^{-1} \sum_i \left\{ f(x_i) \left[p_0 y_i + \sum_j p_j (y_{i-j} + y_{i+j}) \right] \right\} \quad . \quad (14)$$

This equation can be expanded and rearranged to obtain

$$\begin{aligned} a_{sm} = & \sum_k F_{mk}^{-1} \sum_i \left[p_0 f_k(x_i) + \sum_j p_j f_k(x_{i-j}) \right. \\ & \left. + \sum_j p_j f_k(x_{i+j}) \right] y_i + \text{residual terms.} \end{aligned} \quad (15)$$

Let $f_{sk}(x_i) = p_0 f_k(x_i) + \sum_j p_j f_k(x_{i-j}) + \sum_j p_j f_k(x_{i+j})$. Thus one can write

$$a_{sm} = \sum_k F_{mk}^{-1} \left[\sum_i f_{sk}(x_i) y_i + \text{residual terms} \right] . \quad (16)$$

It can be shown that the sum of the residual terms is small because the number of channels used in the smoothing, $2q + 1$, is generally much smaller than I . Moreover, it consists of equal numbers of positive and negative terms.

One can, therefore, approximate a_{sm} by

$$a_{sm} \cong \sum_k F_{mk}^{-1} \sum_i \left[f_{sk}(x_i) y_i \right] . \quad (17)$$

Now that a_{sm} is written in terms y_i , we can write the square of the deviation of a_{sm} in terms of the deviations of the y_i :

$$\sigma_{a_{sm}}^2 = \sigma_y^2 \sum_l \sum_k F_{ml}^{-1} F_{mk}^{-1} \sum_i f_{sl}(x_i) f_{sk}(x_i) . \quad (18)$$

We now wish to compare $\sigma_{a_{sm}}^2$ with $\sigma_{a_m}^2$ to see if the former is less than the latter, i.e., to see if smoothing reduces the deviations in the estimates of the a_{om} .

The functions $f_k(x_i)$ are usually taken to be smooth functions with no discontinuities. In such cases the smoothing of these functions will not change them appreciably:

$$\sum_i f_{s\ell}(x_i) f_{sm}(x_i) \cong \sum_i f_{\ell}(x_i) f_m(x_i). \quad (19)$$

Using this approximation,

$$\sigma_{a_{sm}}^2 \cong \sigma_y^2 F_{mm}^{-1} = \sigma_{a_m}^2. \quad (20)$$

Therefore, smoothing does not increase or decrease the deviations in the estimates of the parameters a_{om} . This conclusion, of course, is valid only if the assumptions and the approximations upon which it is based are valid. Restating these assumptions and approximation:

1. The experimental data y_i are statistically independent and have equal deviations, σ_y .
2. The functions $f_m(x)$ are smoothly varying with no discontinuities.
3. The summation $\sum_i f_k(x_i) \left[p_0 y_i + \sum_j p_j (y_{i-j} + y_{i+j}) \right]$ can be replaced by $\sum_i y_i \left\{ p_0 f_k(x_i) + \sum_j p_j \left[f_k(x_{i-j}) + f_k(x_{i+j}) \right] \right\}$.

Restating the conclusion, the use of smoothed data rather than raw data in analyses by such programs as GAUST does not reduce the deviations in the estimates of such parameters as peak area. Therefore, the usefulness of this type of smoothing appears to be limited to aiding the visual inspection of the data since the statistical fluctuation can be significantly reduced.

IIT RESEARCH INSTITUTE

VI. DEVELOPMENT OF THE COMBINED-NEUTRON-EXPERIMENT
DETECTOR PROBE

IIT Research Institute was assigned the task of designing and fabricating the probe to be used with the neutron generator built by the SANDIA Corp. To accomplish this task, decisions were made concerning various experimental parameters. These included choosing a suitable material and shape for the fast-neutron shadow shield, determining the reflector thickness necessary to obtain good capture gamma-ray spectra, and determining whether shielding would be necessary to eliminate electromagnetic interference.

These initial studies are complete⁽¹⁴⁾ and are summarized below. The probe has been designed and fabricated, and capture gamma-ray, cyclic activation, and inelastic spectra have been obtained.

A. Selection of the Fast-Neutron Shadow Shield Material

The first screening of possible shield materials was based on the fast-neutron-removal cross section. For a minimum length shield, the macroscopic-removal cross section (Σ_r) should be large. However, for a minimum weight shield, the mass absorption coefficient (μ_r) should be large. As a compromise between weight and length considerations, the product $\mu_r \Sigma_r$ was used as a measure of a material's desirability.

Four other characteristics were then examined for each of the elements. These were (1) fast-neutron activation, (2) thermal neutron activation, (3) thermal neutron capture gamma-ray production, and (4) gamma-ray absorption at 2 MeV.

No one material was found to be ideal. Nickel, ruthenium, zinc, and molybdenum emerged as the four most promising materials. Nickel was eliminated on the basis of its somewhat large capture gamma-ray production rate. Ruthenium is not readily available and zinc is activated more readily by fast neutrons. Molybdenum was chosen as a possible compromise material that would not be objectionable to any of the techniques in the combined neutron experiment.

B. Reflector Thickness

The probe has been designed and constructed to provide reflector thicknesses of 0, 4, and 8 cm. Before a final decision can be made regarding the neutron reflector thickness, experimentation will be necessary in which all three thicknesses will be used in conjunction with the three models - basalt, dunite, and granite.

C. The Detector Shield Assembly

The probe provides a can-shaped assembly to house the 3 in. x 3 in. NaI(Tl) detector. The inner diameter of this can is 3.875 in., which should be adequate for the space qualified

detector (its diameter is not expected to exceed 3.79 in.) Thermal neutron shielding of the detector is provided by 50 mg/cm² of lithium-6 (about 99 percent attenuation for thermal neutrons) in the form of lithium fluoride which is contained in the walls and end of this assembly. A removable graded shield consisting of 0.125 in. of lead and 0.062 in. of tin is available for around the detector. With this shield in place, virtually all gamma rays and X-rays with energies below 200 keV are attenuated.

D. The Sandia Neutron Generator

The Sandia Generator designated type 26C (Figure 6-1) was received in February 1968. The unit was tested in both the low-frequency high-output mode and the high-frequency low-output mode to determine the operating characteristics of the generator and its acceptibility for the capture gamma-ray experiment.

In the low-frequency high-output mode, neutron production per pulse in excess of 8000 was readily attainable with virtually no neutron production between pulses. The pulse rate was varied from 400 to 500 pulses per second with no apparent affect on the neutron production per pulse. Stable operation was attainable down to about 1000 neutrons per pulse.

In the high-frequency low-output mode a neutron production per pulse of 1000 was attainable again with virtually no neutron production between pulses. The pulse rate was varied from 1000 to 5000 pulses per second with no apparent affect on the neutron production per pulse. Stable operation was attainable down to about 200 neutrons per pulse.

It was found, however, that the voltage multiplier in the SANDIA neutron generator produced electromagnetic interference which degraded the spectral data. Shielding of the generator, the crystal preamplifier, and the photomultiplier tube with electromagnetic shielding material was found to eliminate this interference. In the probe, the photomultiplier tube, the preamplifier, and the neutron generator are all shielded with electromagnetic shielding material.

E. General Probe Configuration

Since the thickness of the hydrogenous neutron reflector material to be used is still uncertain, the basic geometry of the probe was designed to accommodate both a 4-cm- and an 8-cm-thick polyethylene reflector. A general view of the probe with no reflector is shown in Figure 6-3.

The direct shield interposes 6.5 in. of molybdenum between the neutron source and the crystal. This provides the

same total neutron removal cross section as 6 in. of copper. A cylindrical shape is used for the back 4.5-in. portion of the direct shield to absorb the hydrogen capture gamma rays produced in the lucite and oil contained in the neutron generator. For 2-MeV gammas, the transmission of 4.5 in. of molybdenum is less than 1 percent or about the same as that of 3.25 in. of lead.

The centerline of the probe is $2 \frac{5}{8}$ in. from the sample surface. This dimension is determined by the overall size of the shielded NaI crystal which rests almost on the sample surface. The distance from the neutron source to the center of the crystal is $11 \frac{1}{4}$ in.

F. Weight of the Prototype Detector Probe

The weight of the probe, including the neutron generator and 3 in. x 3 in. NaI(Tl) detector, in the three configurations is:

1. Without Reflector - 52 Pounds
2. With the 4-cm Reflector - 65 Pounds
3. With the 8-cm Reflector - 86 Pounds

G. Data Acquisition Using the Probe

A series of operational tests of the prototype detector probe were made using the basalt model. Capture gamma-ray, cyclic activation, and inelastic scattering spectra were obtained and compared with the spectra which were obtained using our

standard setup and procedure.

A sample of the capture gamma-ray and cyclic activation spectra is presented in Figure 6-4. These spectra compare favorably with those obtained with our standard configuration (see Figure 4-1). The molybdenum shield effectively removes the hydrogen capture gamma rays produced in the moderator, and no extraneous lines due to molybdenum have been noted in the spectra.

The inelastic scattering spectrum obtained with the probe (Figure 6-5) again compares favorably with the spectrum obtained with our standard configuration (Figure 4-9).

VII. SUMMARY

Substantial improvements in the capture gamma-ray spectra were evident as a direct result of modifications made to electronics used in obtaining the spectra. Degradation in the energy resolution as well as the abnormally high low-energy count rate have been eliminated.

Capture gamma-ray, cyclic activation, and inelastic scatter spectra were obtained for samples of basalt and granite. An effort made to modify the experimental procedures to permit the detection of hydrogen by the capture gamma-ray technique was successful, and hydrogen was detected in basalt. The table below summarizes those elements that have been identified in the basalt and the granite sample.

Table 7-1

ELEMENT DETECTED IN BASALT AND GRANITE

	<u>H</u>	<u>Fe</u>	<u>Si</u>	<u>O</u>	<u>Al</u>	<u>Ti</u>	<u>Na</u>	<u>Ca</u>	<u>Mg</u>
Basalt	c	c,s	c,a	a,s	s	c	c(?)	c	s
Granite		c	c,a	a	c		c		

c - capture gamma rays

a - cyclic activation

s - inelastic scattering (basalt only)

A prototype of the combined neutron experiment probe has been designed and fabricated. The unit incorporates the Sandia Neutron Generator type 26C, a neutron reflector, a 3 in. x 3 in. NaI(Tl) detector and appropriate neutron and gamma-ray shielding. After an extensive study, molybdenum was selected as a reasonable material for use as a shadow shield. Molybdenum does not appear to interfere significantly, if at all, with any of the experiments in the combined neutron experiment. The capture gamma-ray, cyclic activation, and inelastic spectra obtained using the probe compare well with those obtained with our standard Van de Graaff apparatus.

A considerable effort is being made to apply computer techniques to the analysis of the complex capture gamma-ray spectra. After studying a number of computer programs, Dr. Trombka's approach⁽⁷⁾ appears to be most readily applicable. Unfortunately, the necessary library of response spectra is not complete. In lieu of this code, the areas of individual peaks are being determined using GAUST, a modified version of GAUSS. The inclusion into GAUST of the perturbations to a Gaussian distribution as the result of the Compton edge and first escape peak allows the program to be applied to peaks throughout the energy range of the capture spectrum.

A few spectra (capture plus activation) have been obtained using a small (5 cm³) lithium-drifted germanium detector

in place of the sodium iodide detector. These preliminary runs indicate that this approach holds tremendous potential. Data analysis becomes nearly trivial and the interference between elements is essentially eliminated.

REFERENCES

1. A. L. Turkevich, E. G. Franzgrote, and J. H. Patterson, "Surveyor V Mission Report. Part II: Science Results," Technical Report 32-1246, Jet Propulsion Laboratory, Pasadena, California, 1967.
2. A. L. Turkevich, E. J. Franzgrote, and J. H. Patterson, Science 158, 635 (1967).
3. R. L. Caldwell, W. R. Mills, Jr. L. S., Allen, P. R. Bell, and R. L. Heath, Science 152, 457 (1966).
4. W. R. Mills, Jr., and W. W. Givens, "Neutron Die-Away Experiment for a Lunar and Planetary Analysis," Final Report, Mobile Research Corporation, April 26, 1967.
5. J. H. Reed, "Compositional Analysis of Lunar and Planetary Surfaces Using Neutron Capture Gamma Rays," Report No. IITRI-A6155-5, Annual Report May 1, 1966 to June 30, 1967, IIT Research Institute, Chicago, Ill., 1967.
6. J. W. Mandler and J. H. Reed, "Compositional Analysis of Lunar and Planetary Surfaces Using Neutron Capture Gamma Rays," Report No. IITRI-A6155-6, Quarterly Progress Report July 1, 1967 to September 30, 1967, IIT Research Institute, Chicago, Ill., 1967.
7. J. I. Trombka, "A Numerical Least-Square Method for Resolving Complex Pulse Height Spectra," Report X-641-67-184, Goddard Space Flight Center, NASA, April 1967.

IIT RESEARCH INSTITUTE

8. Unpublished, developed at the Air Force Technical Applications Center.
9. M. Putnam, D. H. Gipson, R. G. Helmer, and R. L. Heath, "A Nonlinear Least-Square Program for the Determination of Parameters of Photopeaks by the Use of a Modified-Gaussian Function," Report IDO-17016, Phillips Petroleum Co., National Reactor Testing Station, USAEC, August 1965.
10. E. T. Whittaker and G. Robinson, The Calculus of Observations Fourth Edition, Blackie and Son Limited, 1944.
11. D. Gibbons and J. Shanks, Report TEES-2671-2, Texas A & M University, 1962.
12. A. Savitzky and M. J. E. Golay, "Smoothing and Differentiation of Data by Simplified Least-Squares Procedures," Analytical Chemistry 36, pp. 1627-1638 (1964).
13. H. P. Yule, "Mathematical Smoothing of Gamma Ray Spectra," Nuclear Instruments and Methods 54, pp. 61-65 (1967).
14. J. W. Mandler, R. A. Semmler and J. H. Reed, "Compositional Analysis of Lunar and Planetary Surfaces Using Neutron Capture Gamma Rays," Report No. IITRI-V6032-8, Quarterly Progress Report January 1, 1968 to March 31, 1968, IIT Research Institute, Chicago, Ill., 1968

APPENDIX

SAMPLES OF THE DIGITAL DATA OBTAINED DURING THE
TEST OF THE COMBINED-NEUTRON-EXPERIMENT PROBE

Data for Figure 6-4(A)

BASALT-Capture Spectrum (using probe and 8 cm polyethylene)

	0	1	2	3	4	5	6	7	8	9
0	0	23988	54668	49333	38707	32858	30435	32474	33352	24771
10	20087	18075	16190	14816	14251	13836	14025	13287	12469	11600
20	11001	10288	9978	9556	8950	8596	8582	8278	8277	7726
30	7376	7181	6868	6533	6913	6992	7035	7007	6508	5720
40	5236	4770	4775	4444	4273	4197	4519	4721	4491	3753
50	3506	3360	3241	3282	3039	2964	2707	2676	2705	2711
60	2819	2859	2692	2479	2232	2122	2171	2154	2085	2015
70	2146	2031	2045	2042	1974	1916	1803	1839	1738	1756
80	1685	1611	1698	1571	1642	1612	1575	1587	1570	1472
90	1461	1417	1396	1440	1404	1389	1322	1336	1282	1313
100	1377	1325	1340	1229	1190	1134	1130	1075	1133	1142
110	1175	1128	1154	1078	1146	1026	1034	1026	952	929
120	1014	928	964	942	939	991	1005	967	1013	945
130	968	871	921	832	817	783	778	792	776	784
140	837	883	902	880	898	840	869	783	855	780
150	789	732	722	741	791	716	808	830	831	793
160	840	833	843	891	940	877	882	815	808	756
170	749	831	926	840	767	782	743	673	711	730
180	714	674	700	664	618	628	624	580	617	610
190	584	607	506	471	502	477	489	505	559	474
200	460	415	385	332	362	368	392	386	400	403
210	402	360	368	336	308	236	222	213	162	149
220	160	164	174	207	197	209	168	166	118	100
230	75	58	65	53	45	50	40	33	37	34
240	45	30	31	27	39	31	41	40	35	30
250	30	24	25	20	20	20				

1808110

Data for Figure 6-4(B)

BASALT-Cyclic Activation Spectrum (using probe and 8 cm polyethylene)

	0	1	2	3	4	5	6	7	8	9
0	0	6977	13993	12137	9699	8204	8254	8722	8528	6532
10	5991	6055	5325	4693	4532	4511	4428	4224	4190	4186
20	4050	3927	3787	3543	3380	3210	3215	3060	3021	2874
30	2721	2581	2436	2286	2160	2214	2611	2958	2968	2156
40	1688	1305	1178	1085	1074	1071	1363	1805	1632	1084
50	760	498	437	402	368	322	340	325	343	354
60	367	351	329	291	262	265	248	228	236	235
70	246	267	355	336	325	276	249	221	235	193
80	165	169	169	184	157	141	142	137	139	156
90	155	141	134	156	135	139	133	153	118	121
100	140	127	119	136	113	136	123	108	103	116
110	115	116	106	95	132	117	94	100	109	92
120	107	83	102	101	101	89	79	99	112	98
130	93	88	95	94	94	96	79	80	94	79
140	102	102	101	101	104	120	129	137	117	134
150	134	127	132	134	122	121	122	113	117	119
160	141	142	190	219	231	201	174	147	139	131
170	95	94	81	74	79	62	75	100	132	130
180	148	127	85	64	46	36	31	33	24	31
190	28	29	23	29	21	25	24	21	18	15
200	7	19	14	16	11	21	15	8	13	21
210	20	15	10	13	9	9	5	7	12	10
220	5	6	3	11	5	4	10	4	7	5
230	3	3	2	3	4	2	2	1	3	5
240	3	1	1	3	5	1	3	3	3	2
250	2	2	1	1	1	1	3	3	3	
										1808120

Data for Figure 6-5

BASALT-Inelastic Spectrum (using probe and 8 cm polyethylene)

	0	1	2	3	4	5	6	7	8	9
0	0	14489	78388	83661	70574	62847	58763	55987	54916	55811
10	41712	33316	32395	31307	29273	26811	26788	26203	24930	23169
20	22282	19240	17873	17918	18118	16820	15570	14901	14127	13278
30	12695	12567	12724	12348	12564	12697	12395	11123	10324	9997
40	9600	9256	9083	8503	8568	8125	8364	9096	9986	9325
50	8225	7178	6763	6517	6272	6236	5953	5731	5878	5775
60	5690	5739	5794	5470	5327	5050	4981	4832	4698	4610
70	4619	4530	4455	4486	4146	4271	4351	4386	4362	4266
80	4209	3995	3787	3699	3608	3624	3660	3545	3543	3566
90	3563	3577	3448	3257	3222	3142	3233	3096	3104	2957
100	2721	2762	2604	2609	2676	2769	2793	2842	2632	2562
110	2484	2527	2473	2388	2360	2221	2074	2025	1993	1985
120	1851	1822	1828	1837	1704	1708	1735	1718	1778	1743
130	1806	1703	1743	1668	1736	1592	1521	1553	1505	1602
140	1487	1526	1517	1434	1523	1550	1650	1673	1755	1693
150	1613	1603	1605	1549	1599	1509	1467	1460	1476	1479
160	1504	1478	1597	1780	1812	1793	1830	1651	1598	1483
170	1453	1352	1373	1303	1247	1202	1289	1196	1417	1429
180	1449	1371	1374	1186	1133	1038	1065	992	1044	991
190	955	964	970	954	911	870	780	759	755	671
200	712	664	687	656	702	640	598	562	604	555
210	507	490	468	399	331	330	339	311	345	340
220	309	264	274	315	242	238	253	225	233	217
230	239	220	252	219	192	188	212	194	181	200
240	184	161	171	173	193	141	173	193	634	2132
250	201	46	65	79	125	164				

1808051

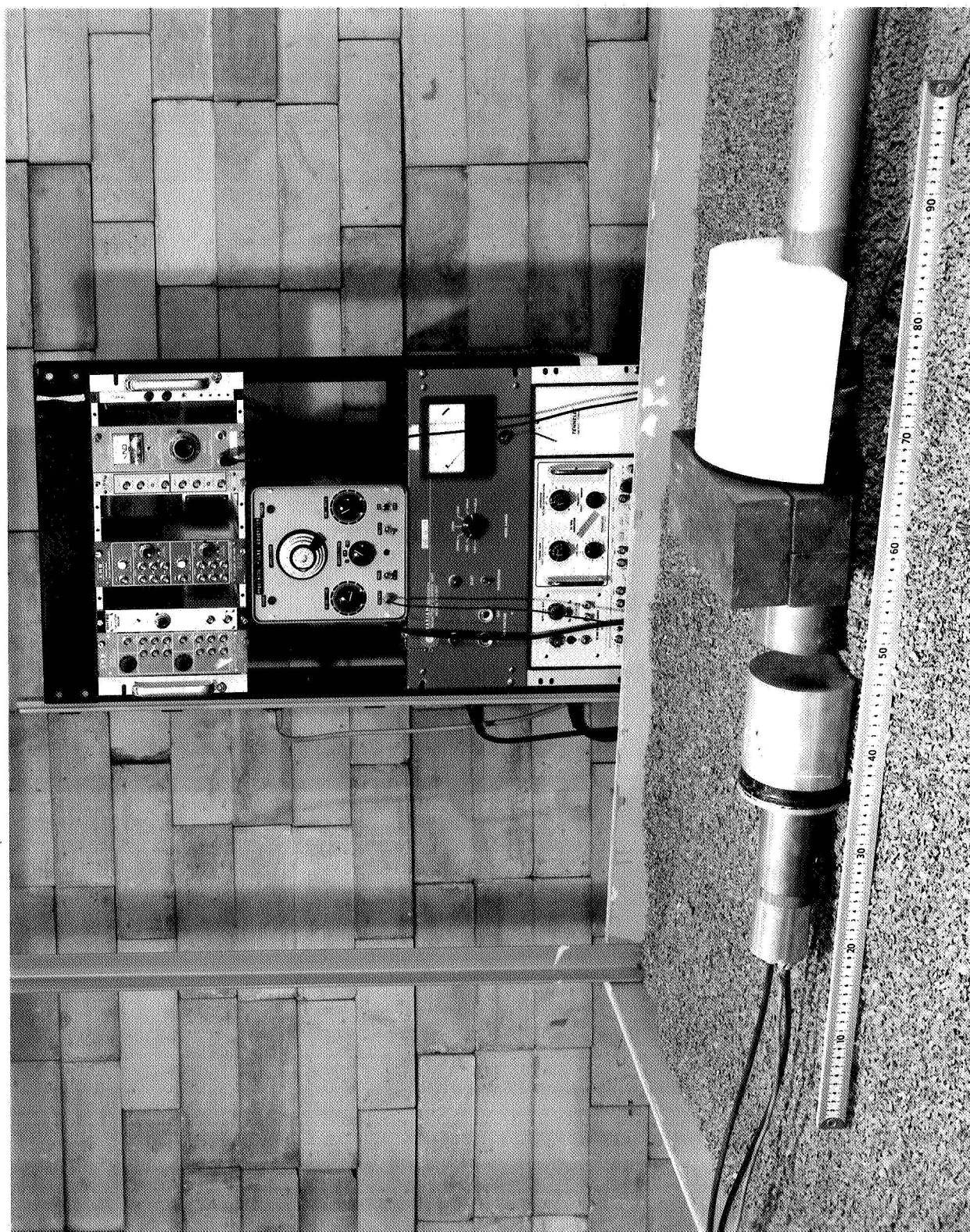


Figure No. 2-1
VIEW OF THE EXPERIMENTAL CONFIGURATION

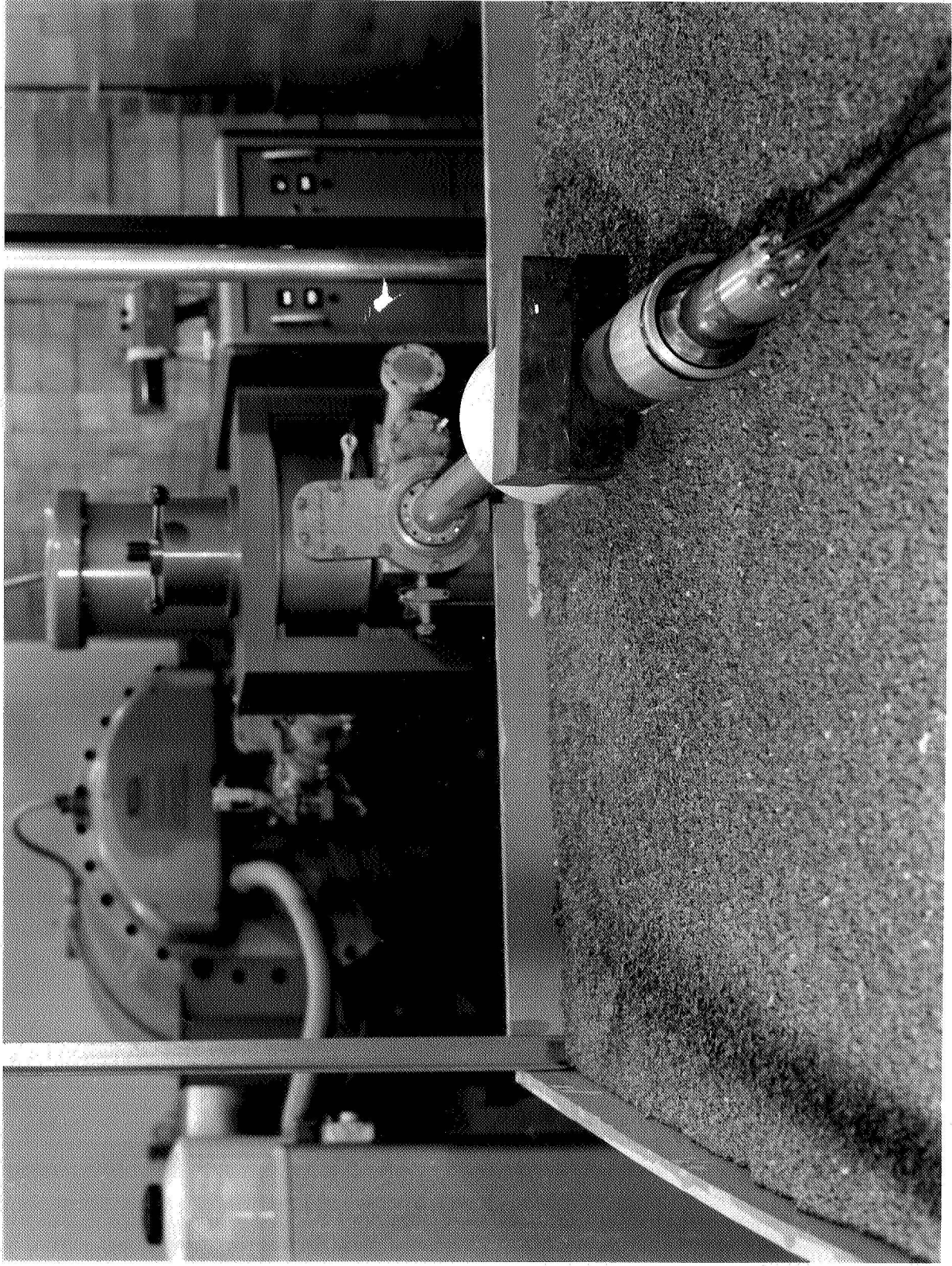


Figure No. 2-2
VIEW OF THE EXPERIMENTAL CONFIGURATION

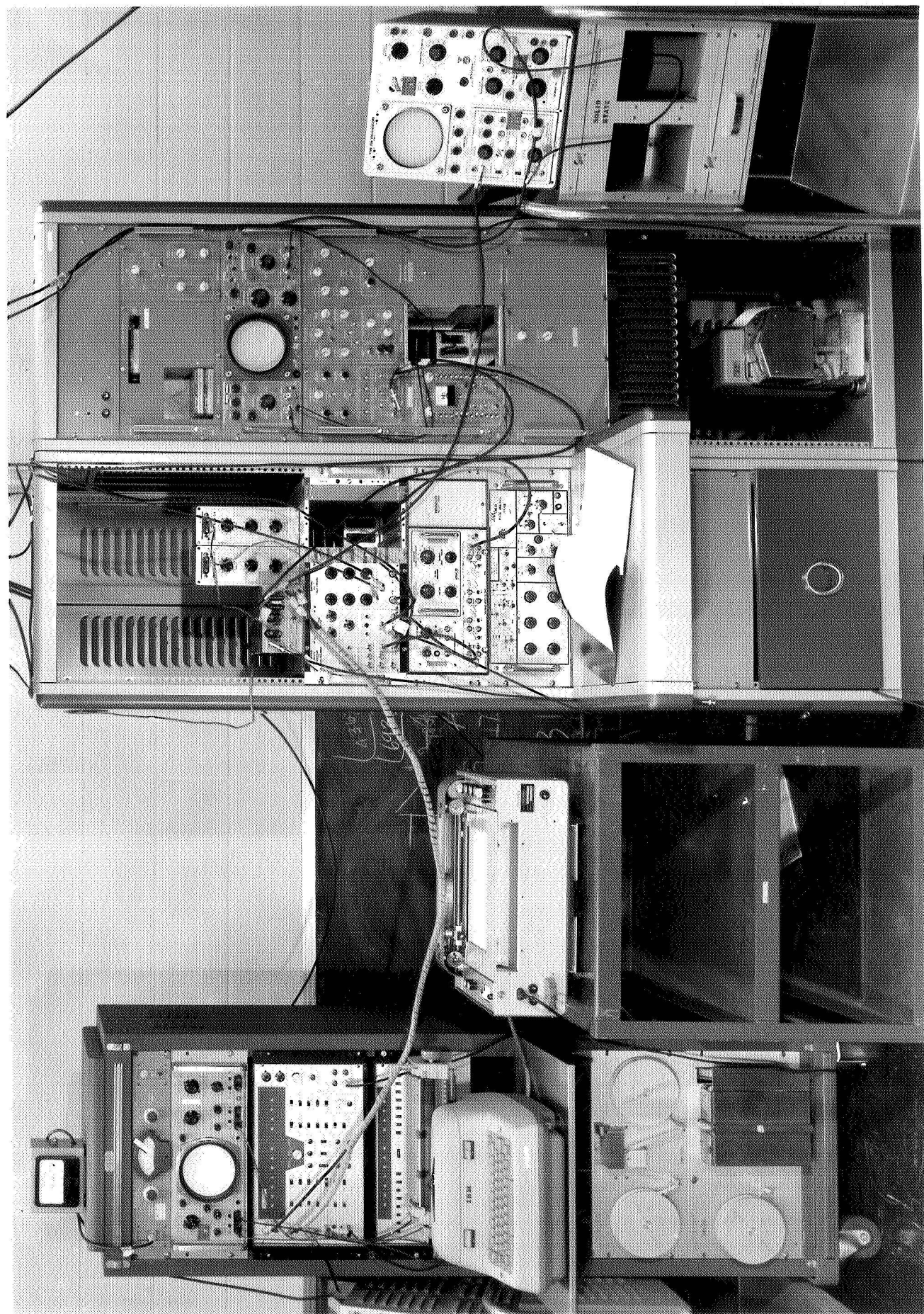


Figure No. 2-3
VIEW OF THE ELECTRONICS

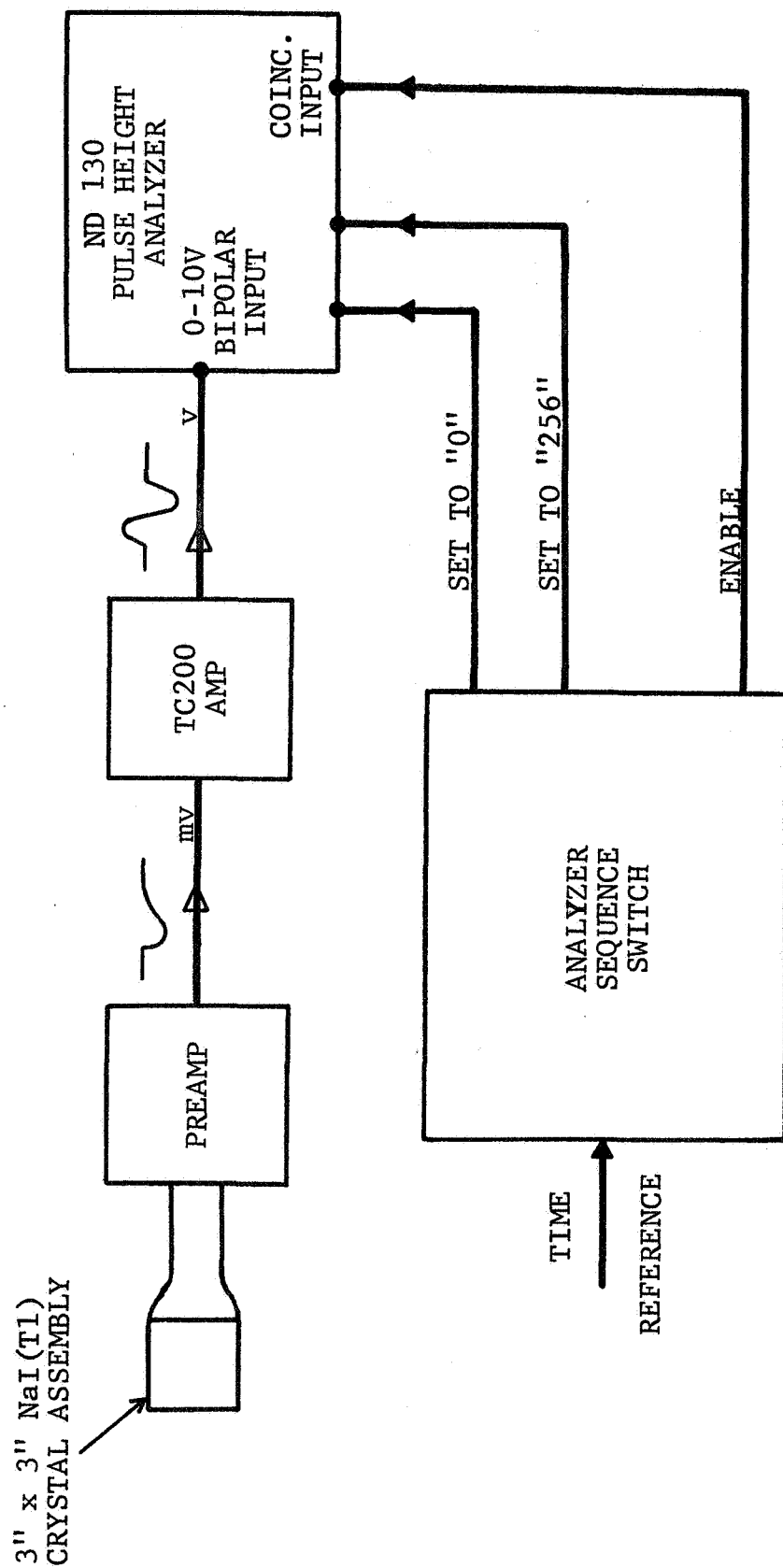
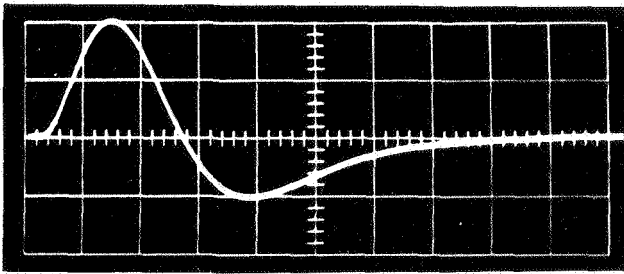


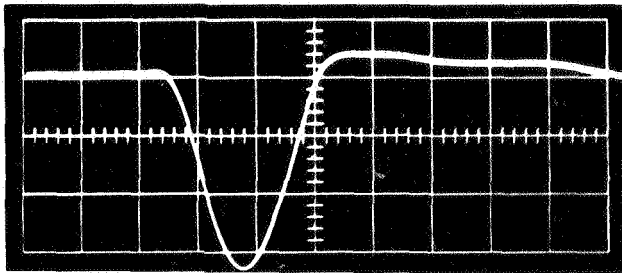
Figure No. 3-1

BLOCK DIAGRAM OF PREVIOUS DATA COLLECTING SYSTEM



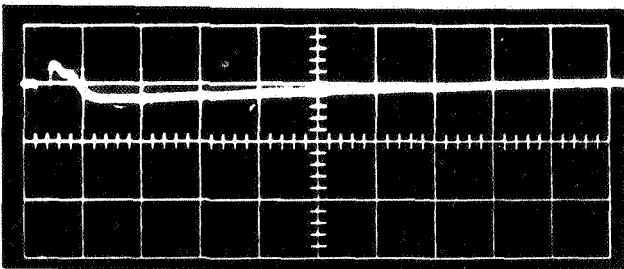
(a) Input to ND 130 Pulse Height Analyzer

Vert. Scale: 5v/div.
 Horiz. Scale: 1 μ sec/div.



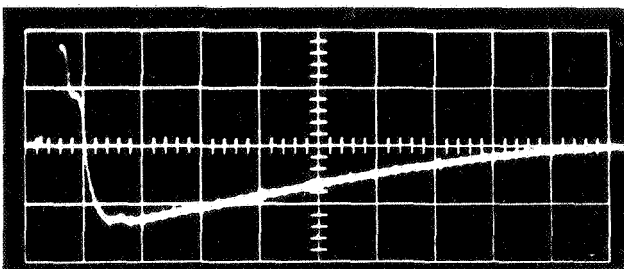
(b) Input to ADC (Actual Pulse to be Analyzed)

Vert. Scale: 0.5v/div.
 Horiz. Scale: 1 μ sec/div.



(c) Input to ADC

Vert. Scale: 0.5v/div.
 Horiz. Scale: 10 μ sec/div.



(d) Input to ADC

Vert. Scale: 0.1v/div.
 Horiz. Scale: 10 μ sec/div.

Figure No. 3-2

OSCILLOSCOPE TRACES OF EFFECTS OF BIPOLAR PULSE ON
 ND-130 PULSE HEIGHT ANALYZER

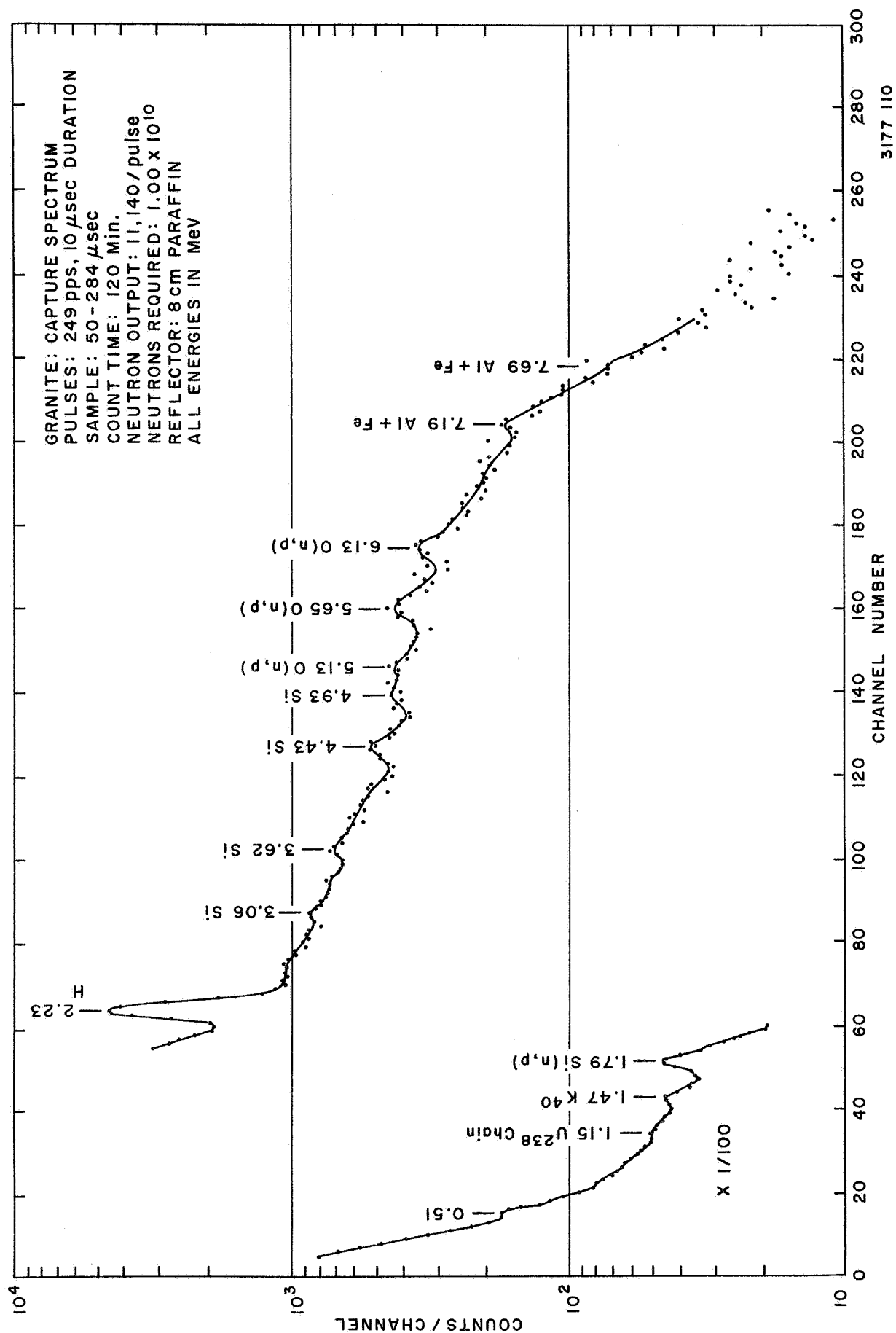


Figure No. 3-5
GRANITE-CAPTURE SPECTRUM (Short Delay - High Output)

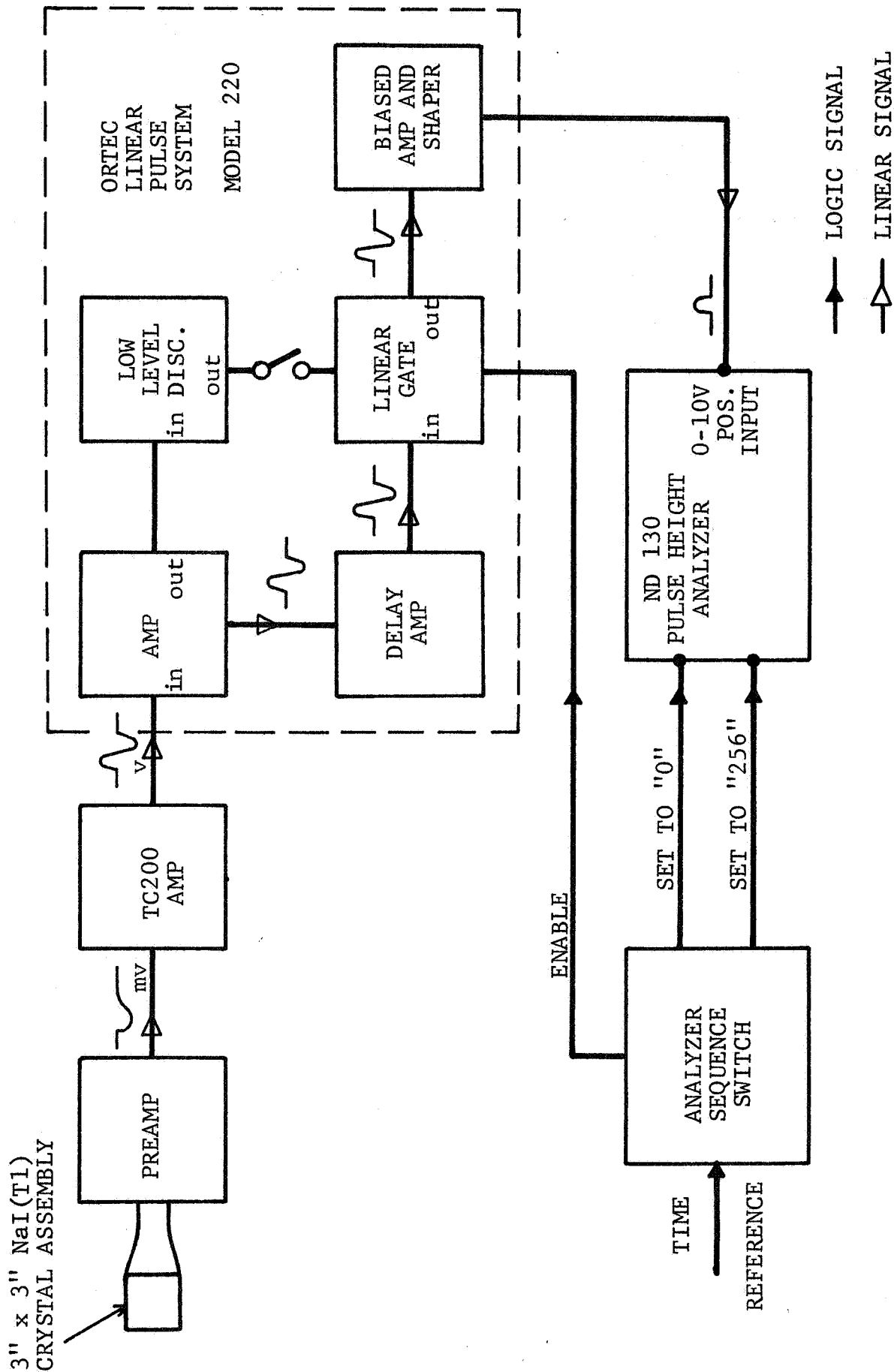


Figure No. 3-4
BLOCK DIAGRAM OF CURRENT DATA COLLECTING SYSTEM

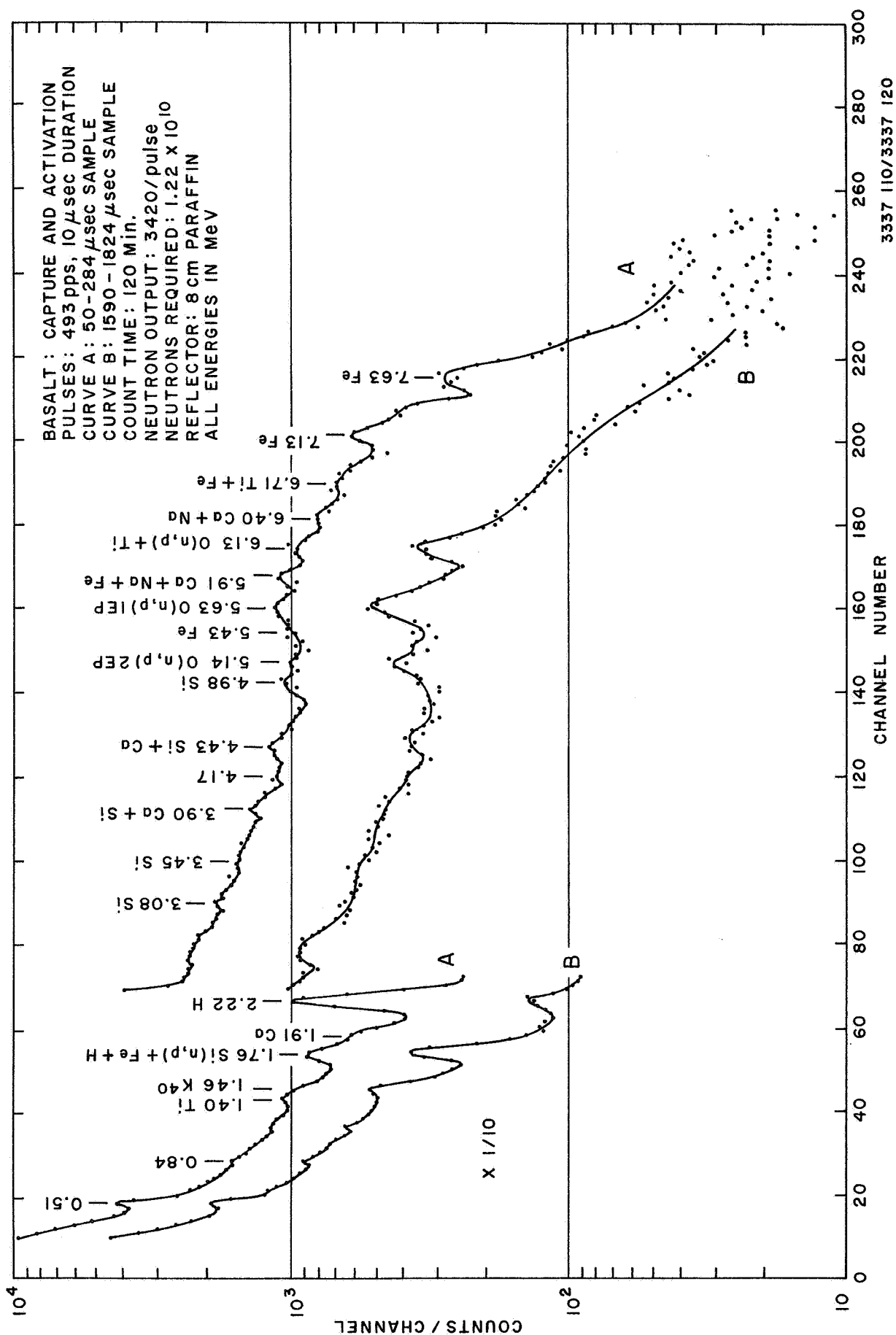


Figure No. 4-1

BASALT-CAPTURE AND CYCLIC ACTIVATION SPECTRA (High Energy)

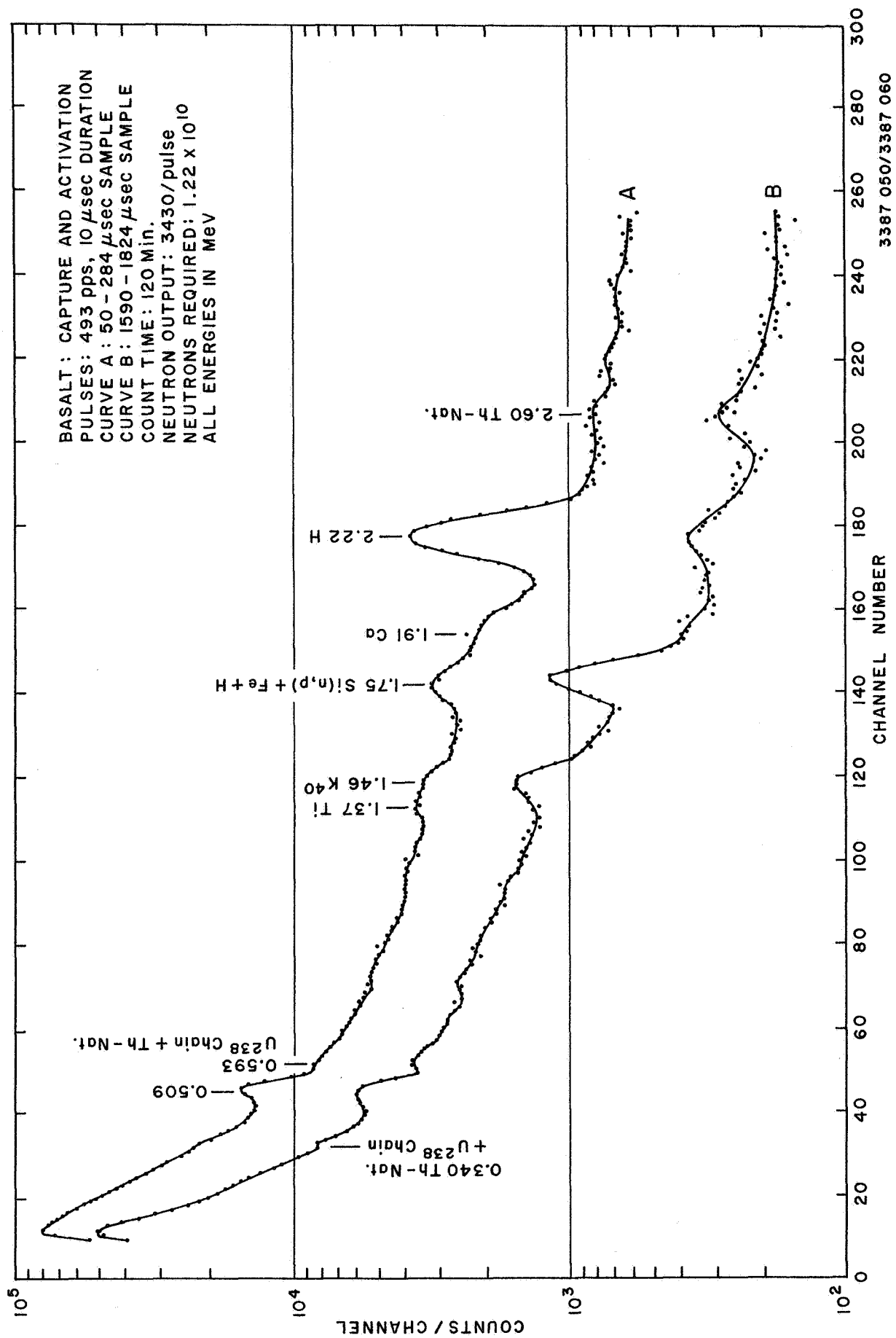


Figure No. 4-2
 BASALT-CAPTURE AND CYCLIC ACTIVATION SPECTRA (Low Energy)

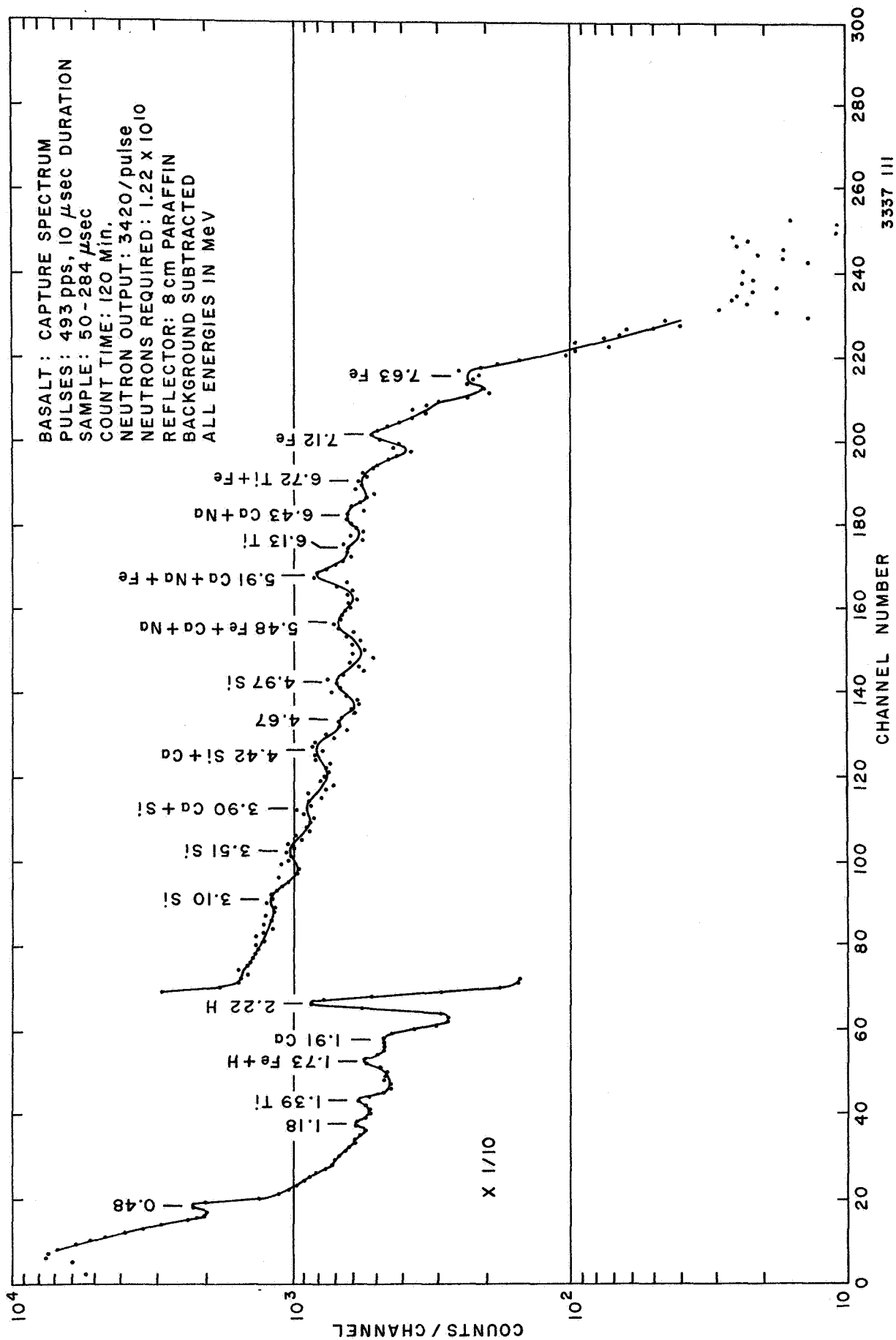


Figure No. 4-3
 BASALT-CAPTURE GAMMA-RAY SPECTRUM (Background Subtracted, High Energy)

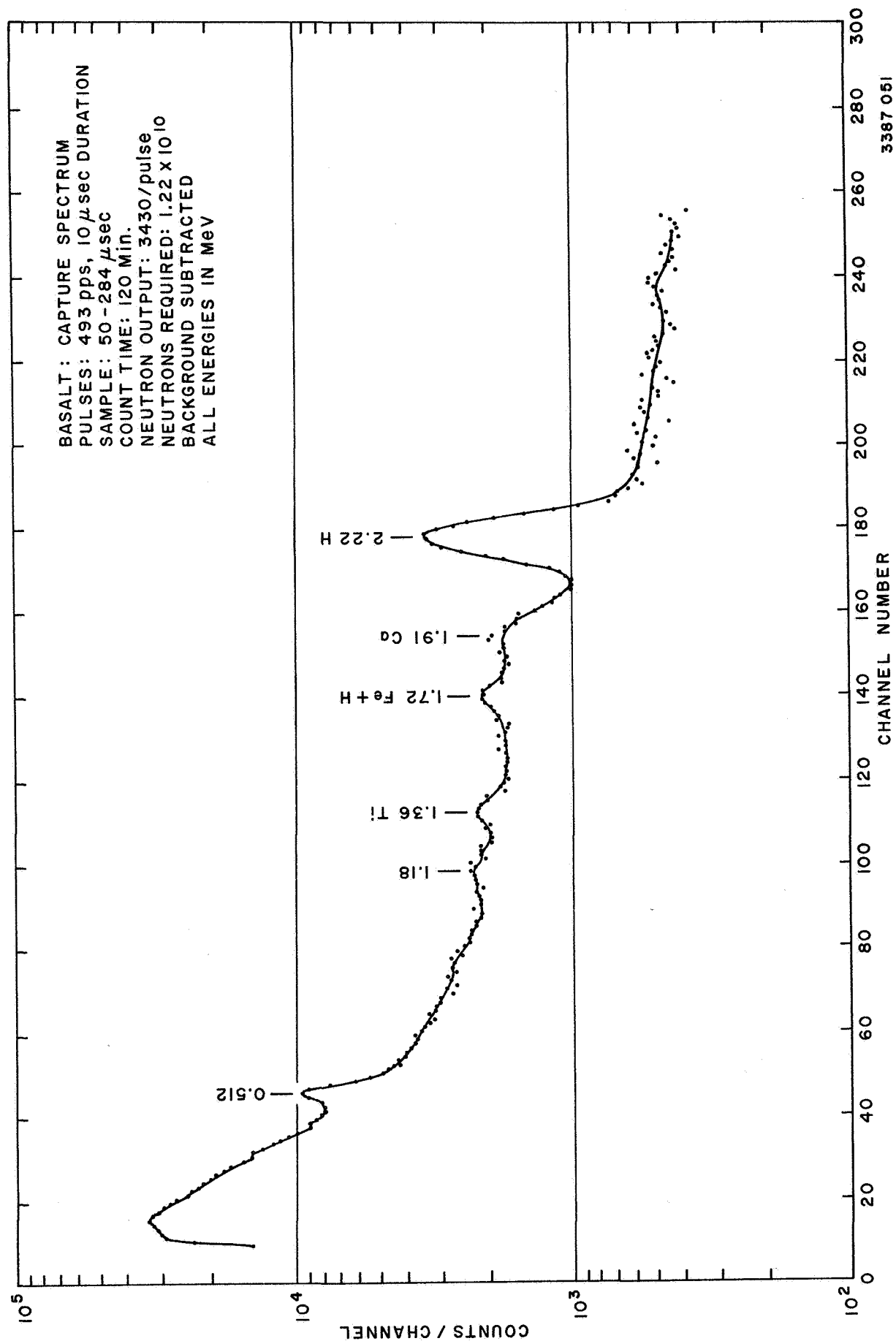


Figure No. 4-4
 BASALT-CAPTURE GAMMA-RAY SPECTRUM (Background Subtracted, Low Energy)

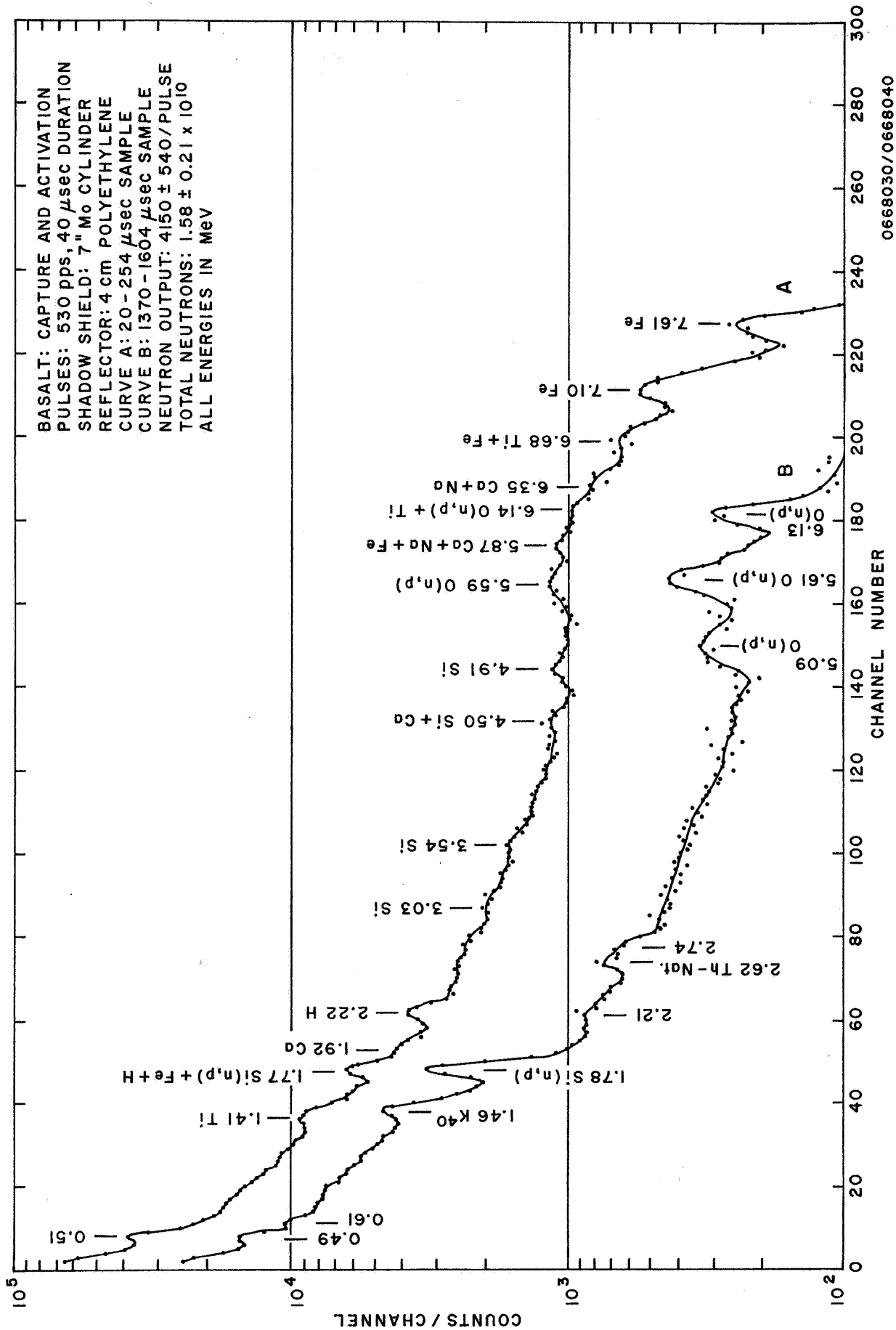


Figure No. 4-5
 BASALT-CAPTURE AND CYCLIC ACTIVATION SPECTRA (4 cm Polyethylene)

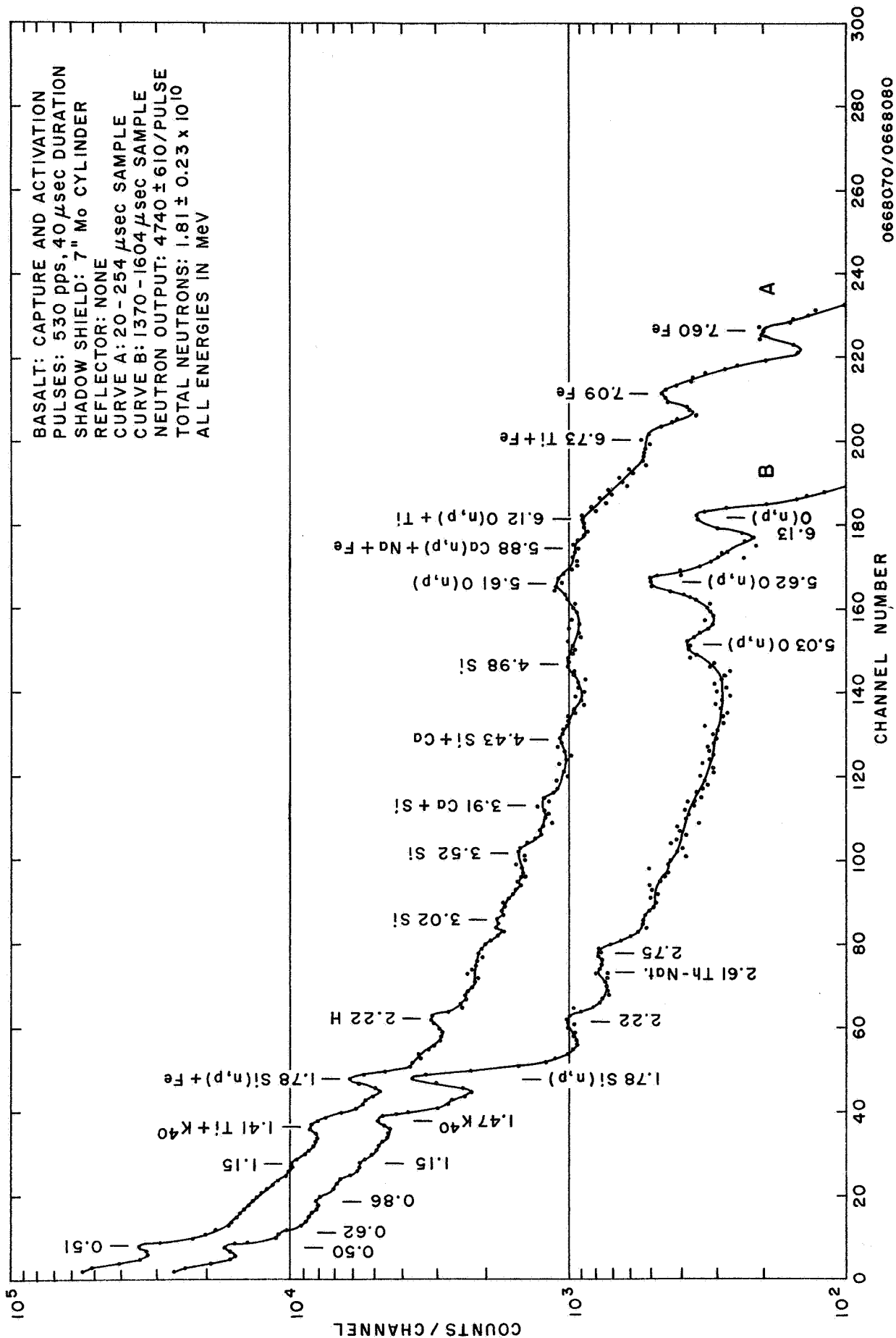


Figure No. 4-6
 BASALT-CAPTURE AND CYCLIC ACTIVATION SPECTRA (No Reflector)

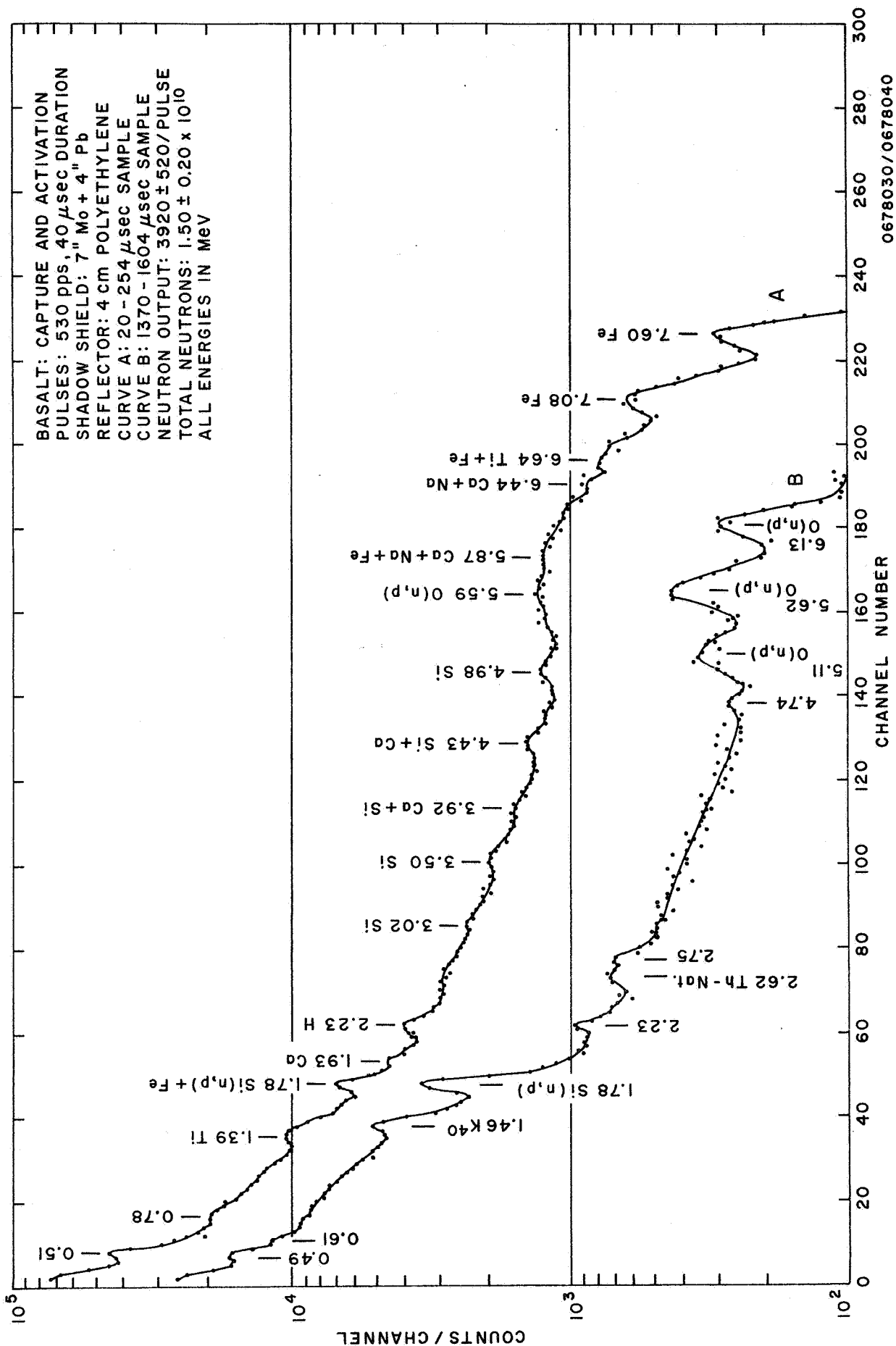


Figure No. 4-7

BASALT-CAPTURE AND CYCLIC ACTIVATION SPECTRA (4 cm Polyethylene with Lead Shield)

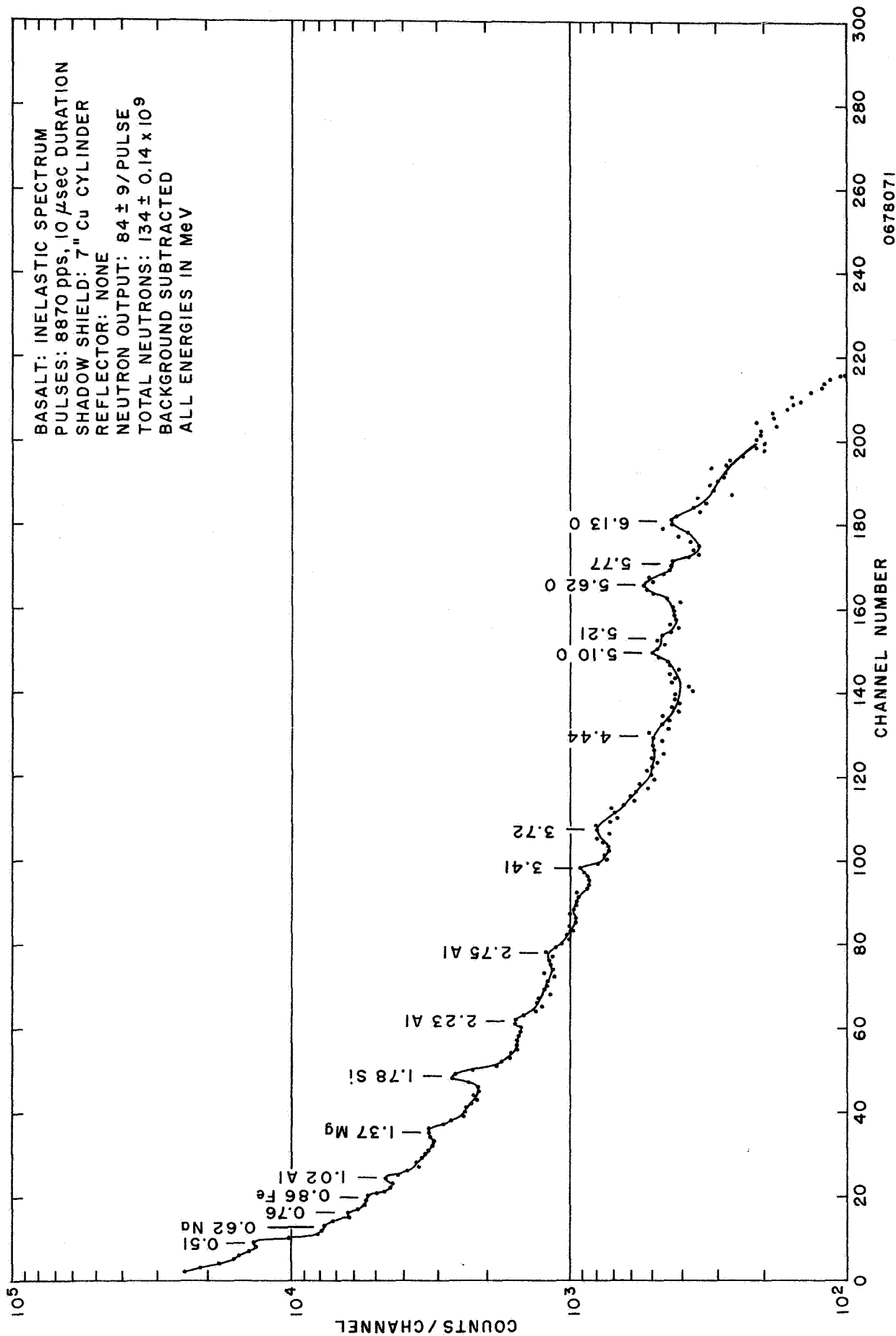


Figure No. 4-8

BASALT-INELASTIC SPECTRUM (No Reflector)

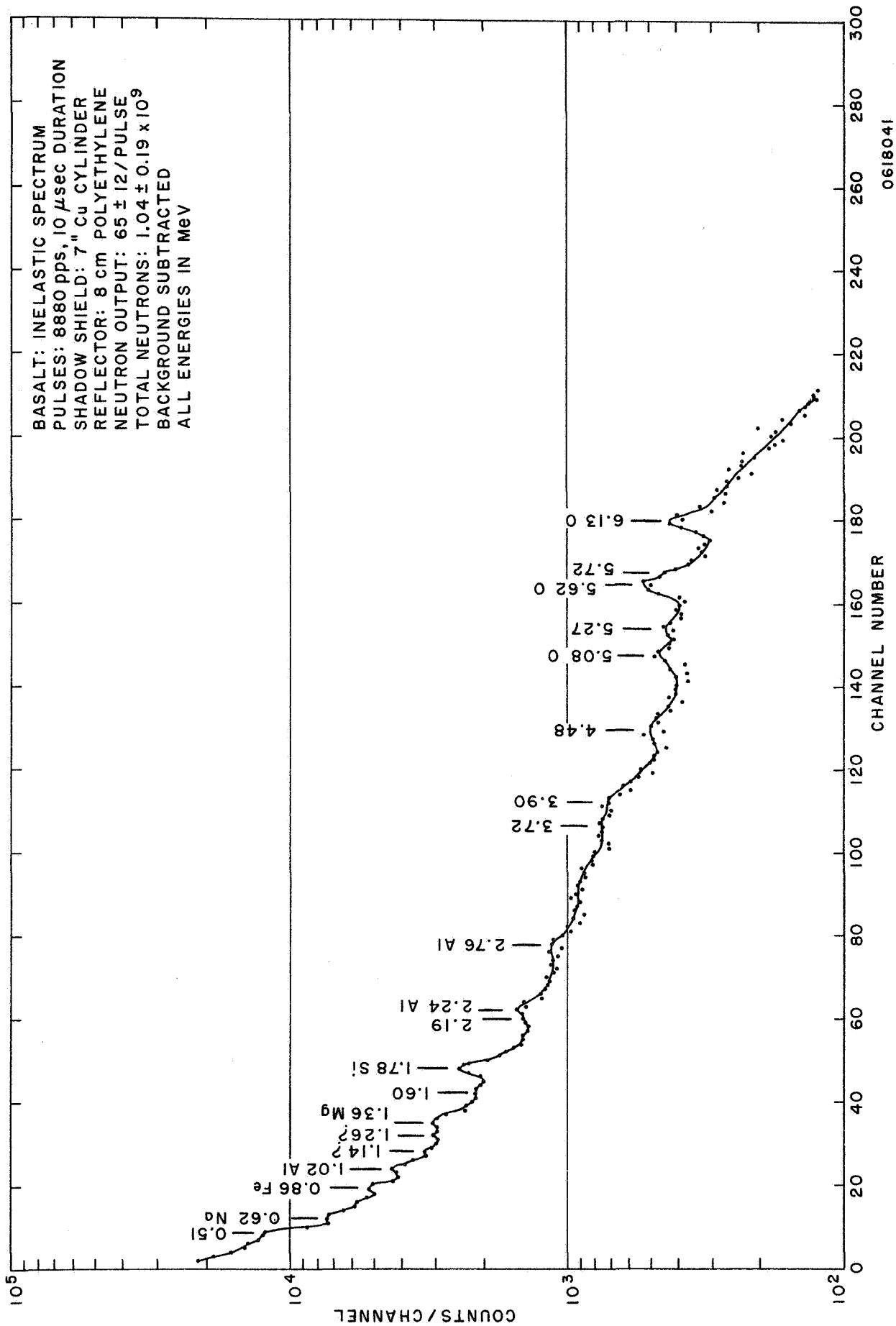


Figure No. 4-9
 BASALT-INELASTIC SPECTRUM (8 cm Polyethylene)

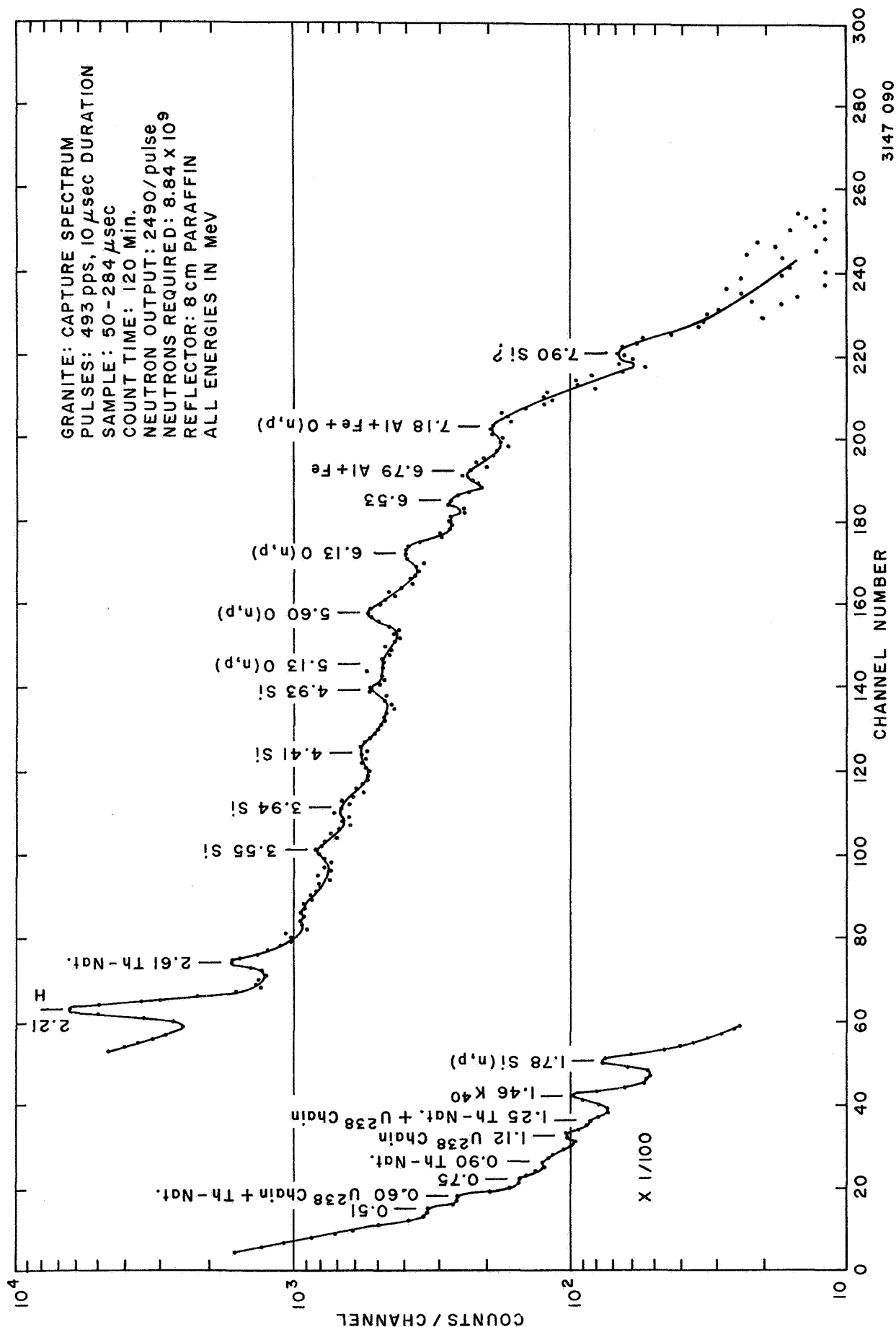


Figure No. 4-10
 GRANITE-CAPTURE SPECTRUM (8 cm Paraffin)

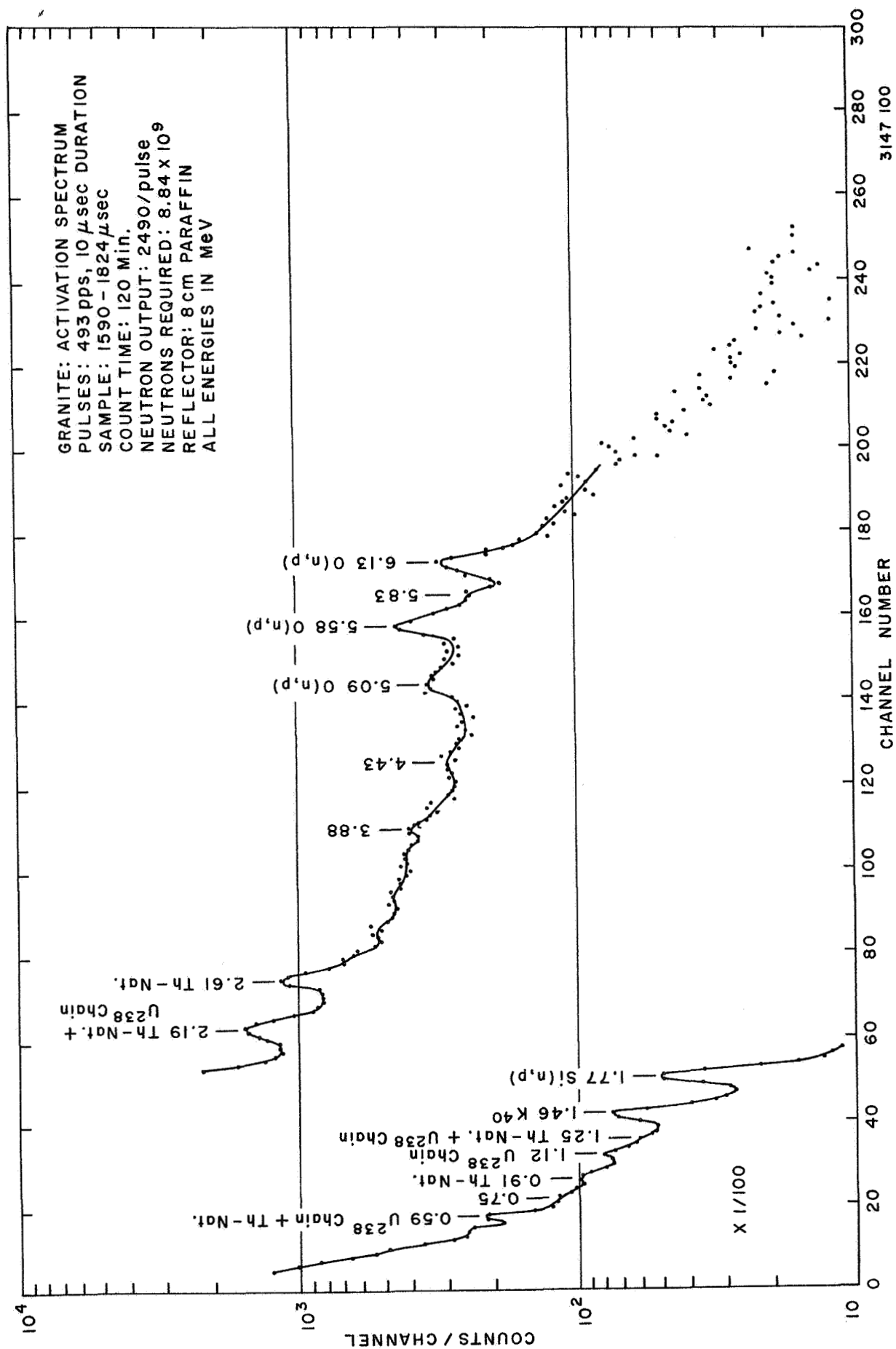


Figure No. 4-11
 GRANITE-CYCLIC ACTIVATION SPECTRUM (8 cm Paraffin)

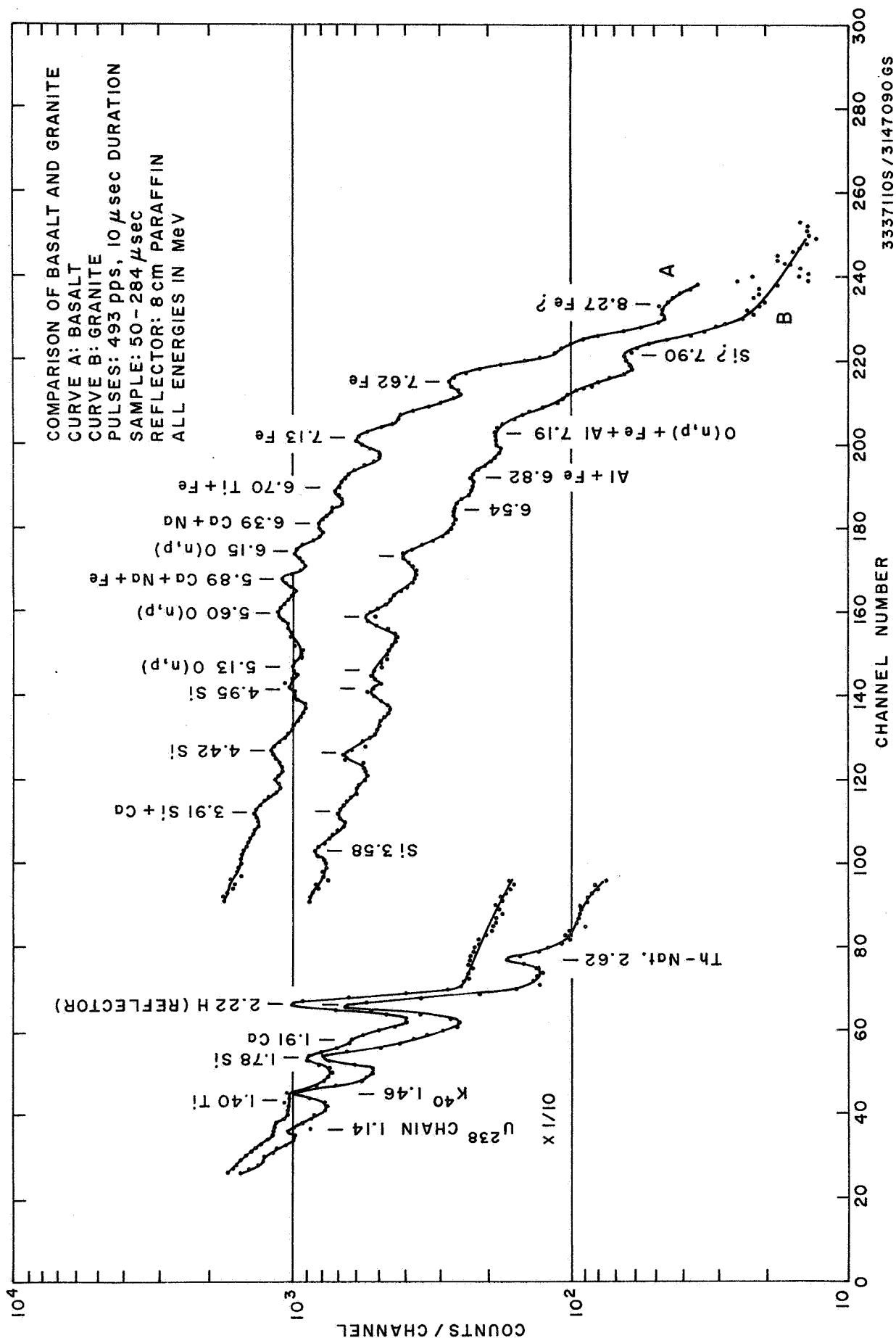


Figure No. 4-12

COMPARISON OF BASALT AND GRANITE

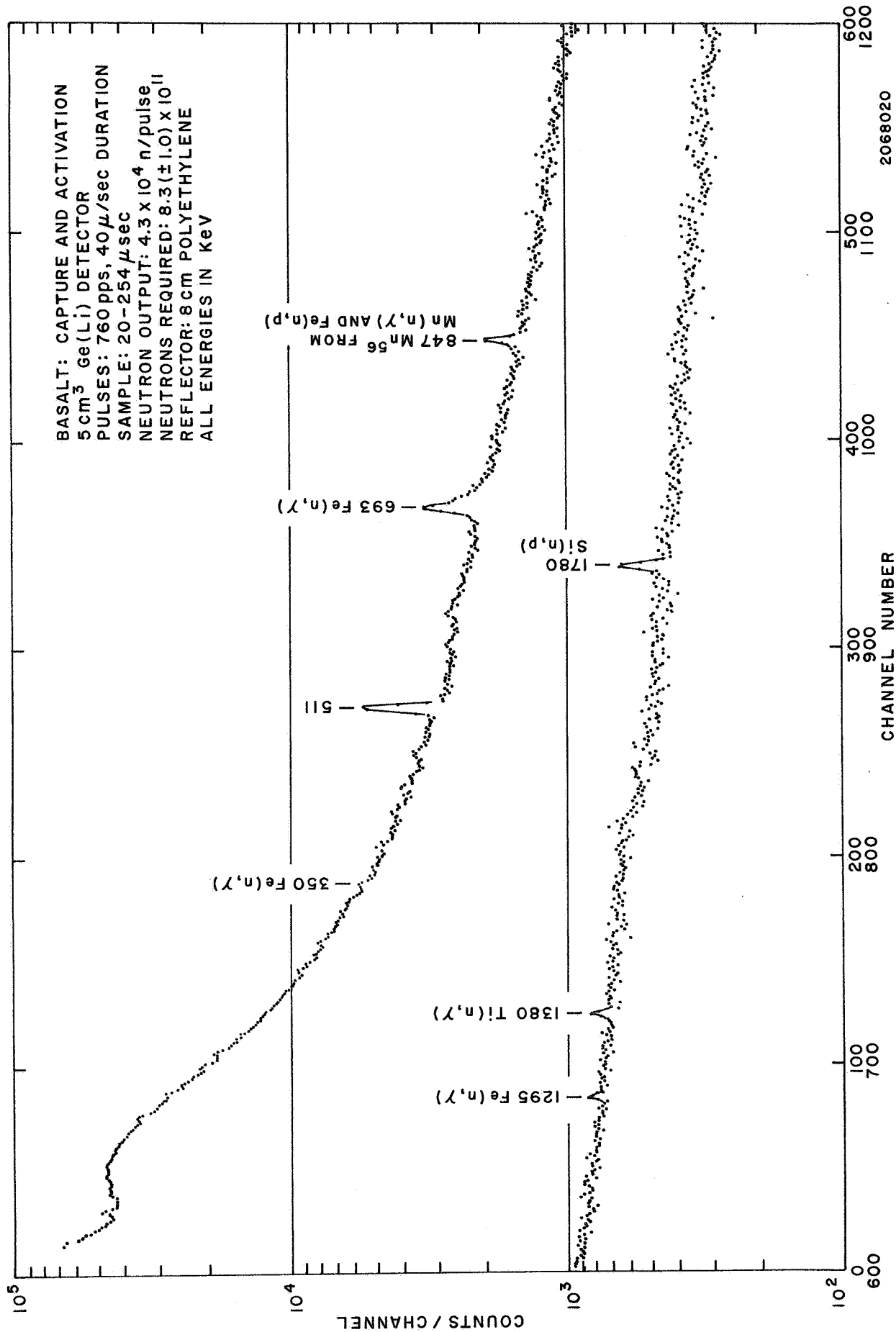
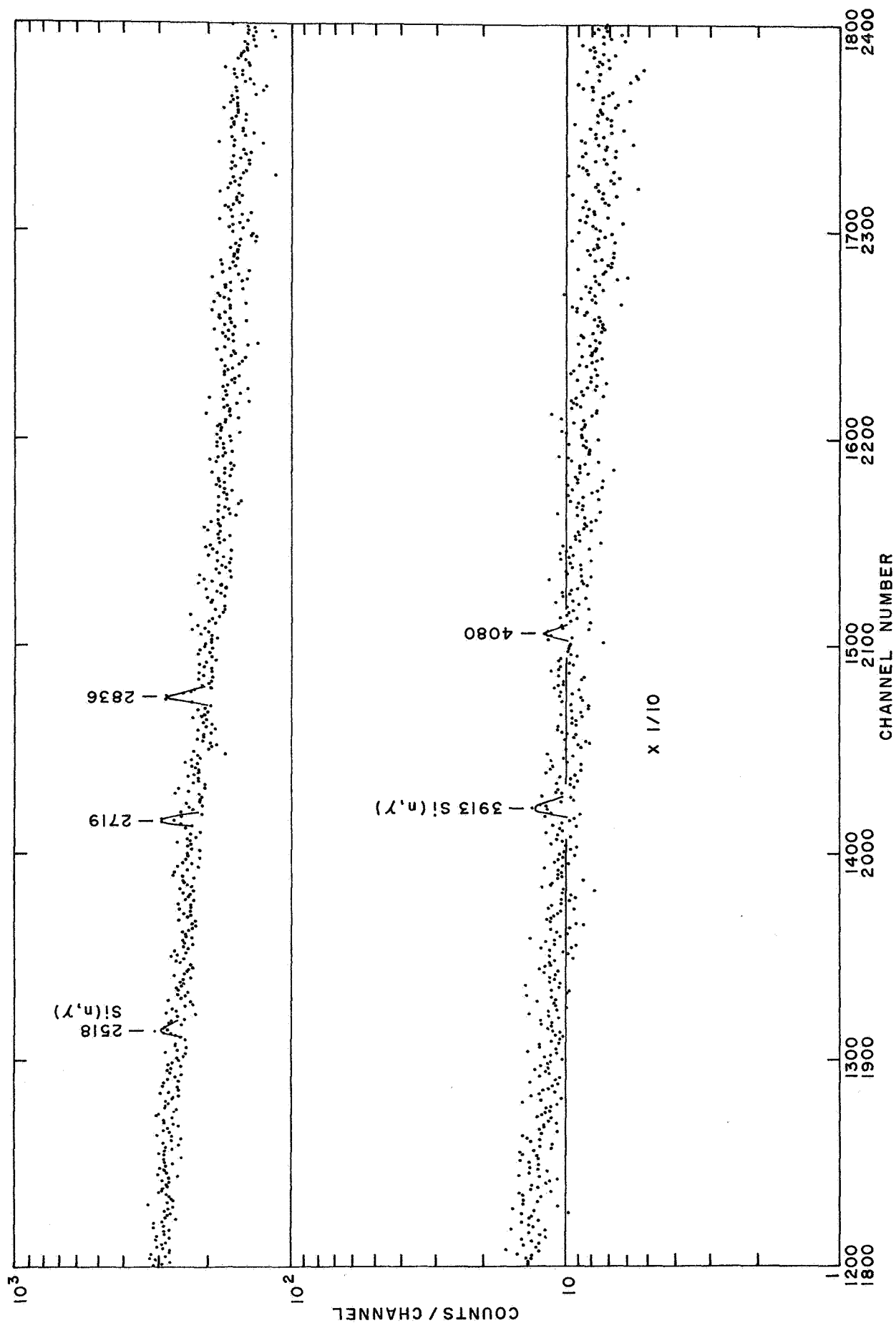
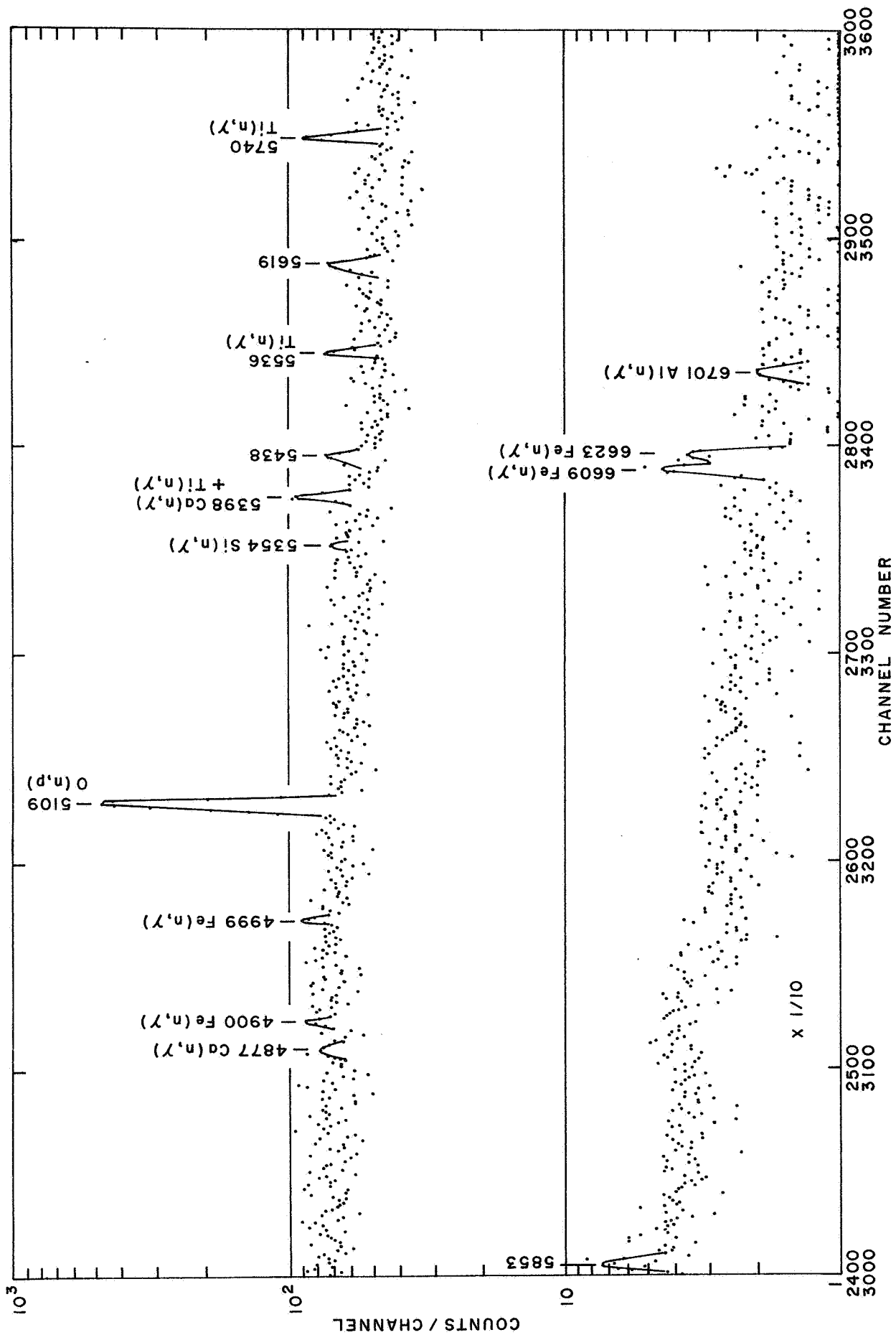


Figure No. 4-13
 BASALT-CAPTURE SPECTRUM (5-cm³ Ge(Li) Detector)





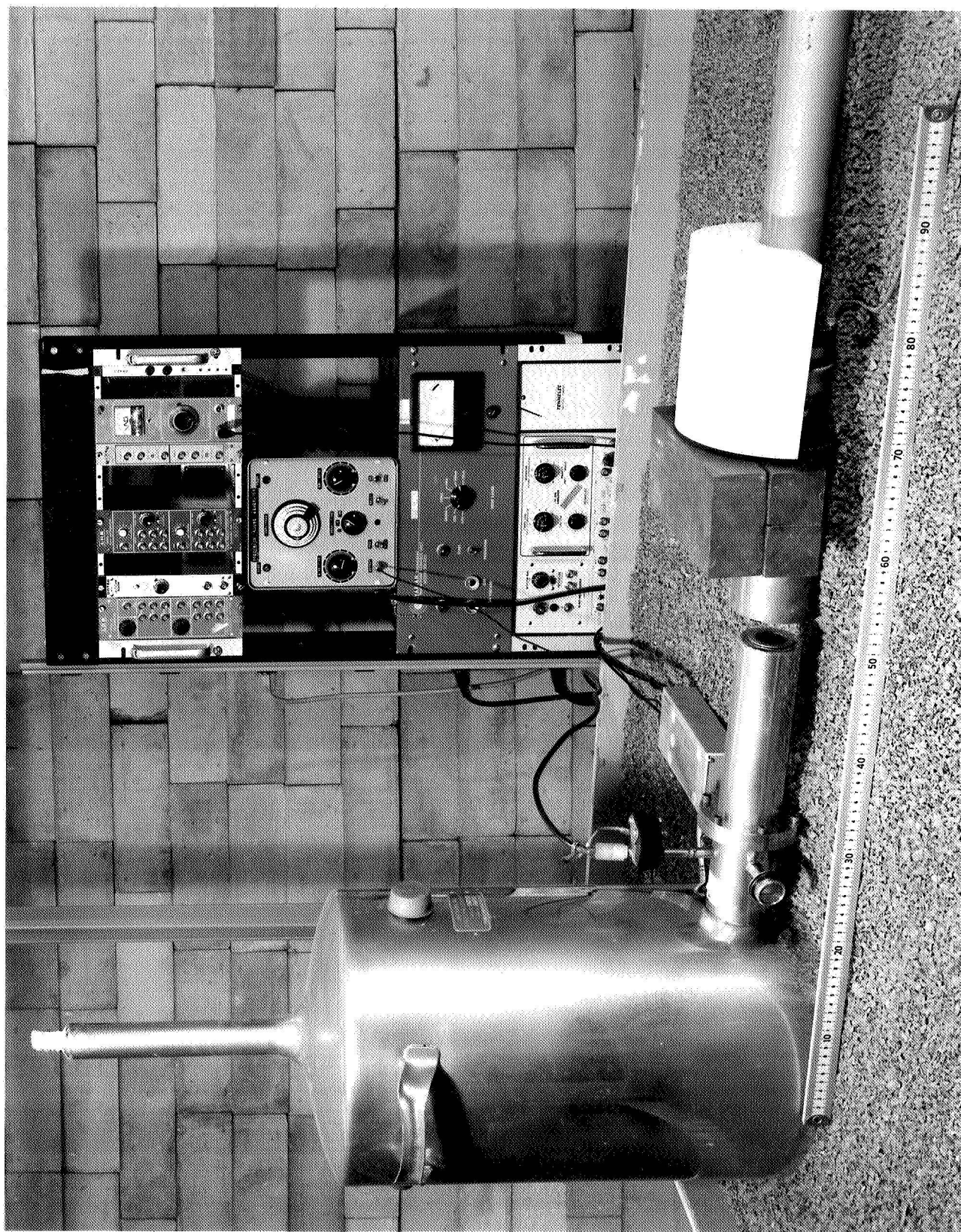


Figure No. 4-14

VIEW OF EXPERIMENTAL CONFIGURATION USING Ge(Li) DETECTOR

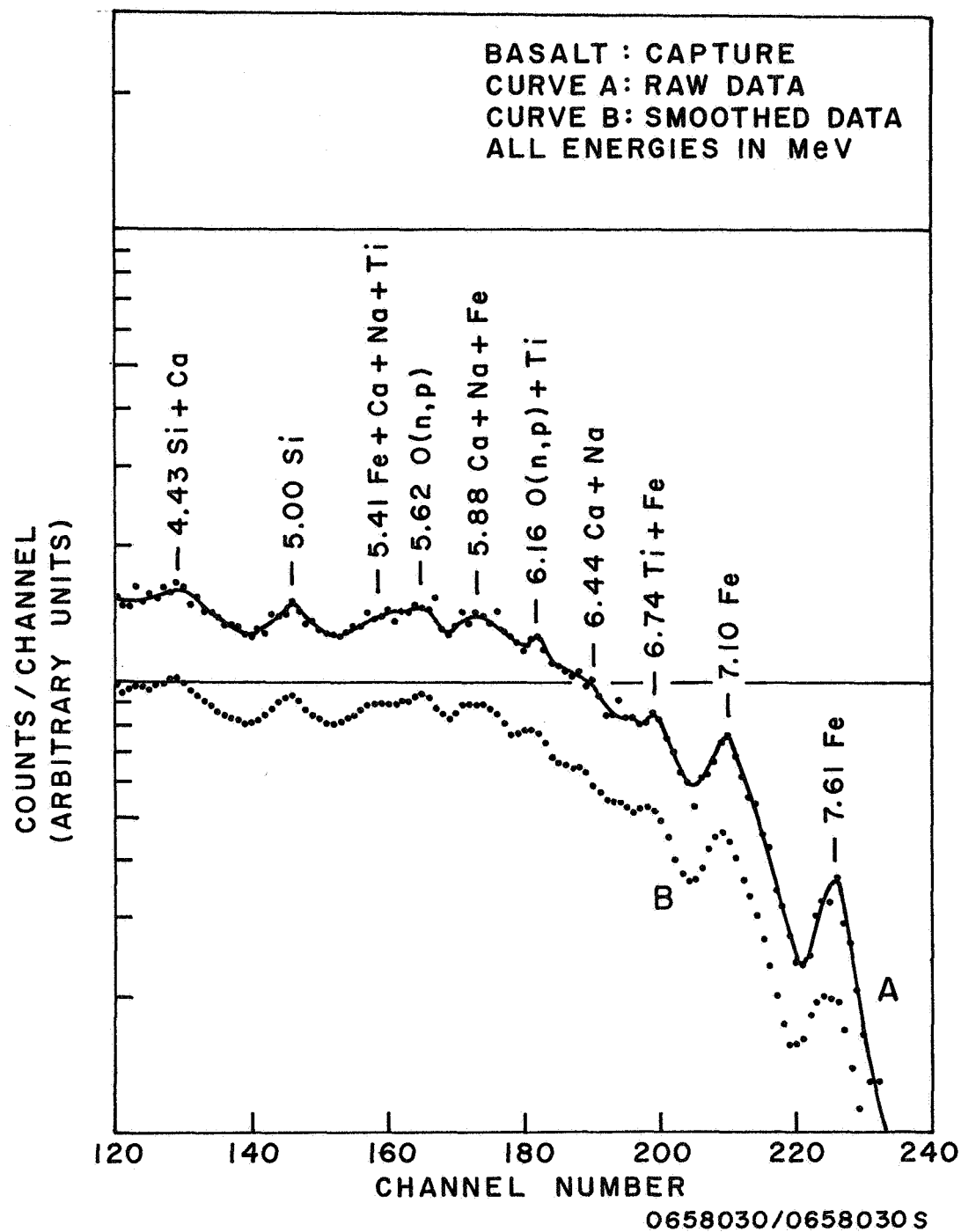


Figure No. 5-1
COMPARISON OF SMOOTHED AND UNSMOOTHED SPECTRUM

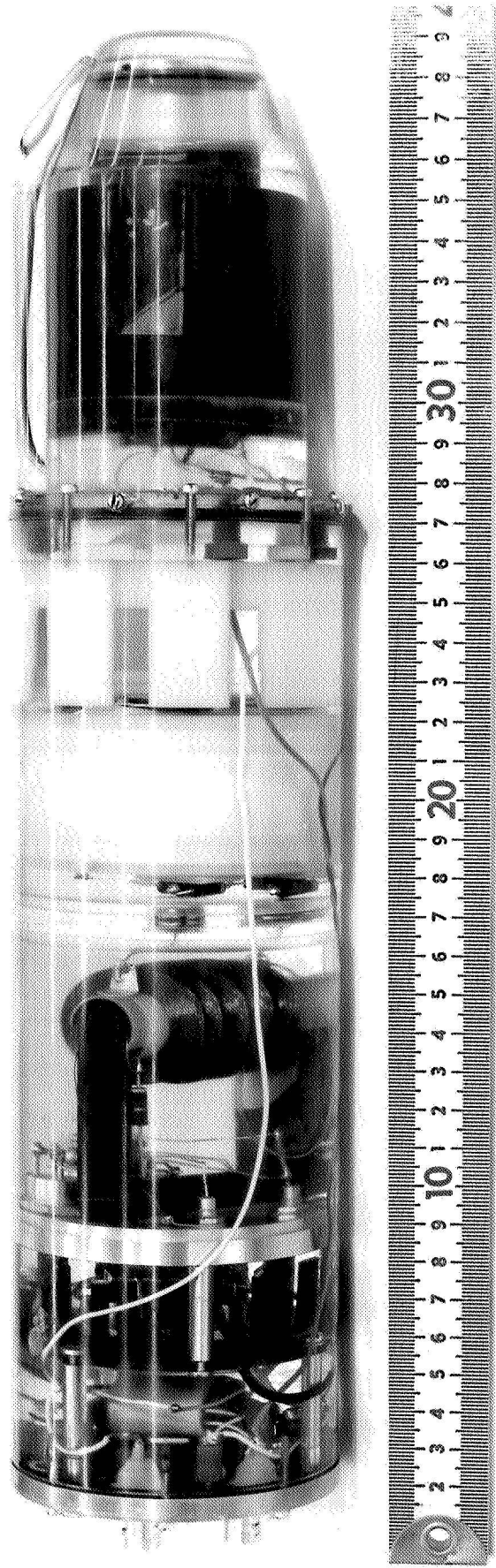


Figure No. 6-1
VIEW OF SANDIA GENERATOR TYPE 26C



Figure No. 6-2

VIEW OF THE COMBINED-NEUTRON-EXPERIMENT DETECTOR PROBE (No Reflector)

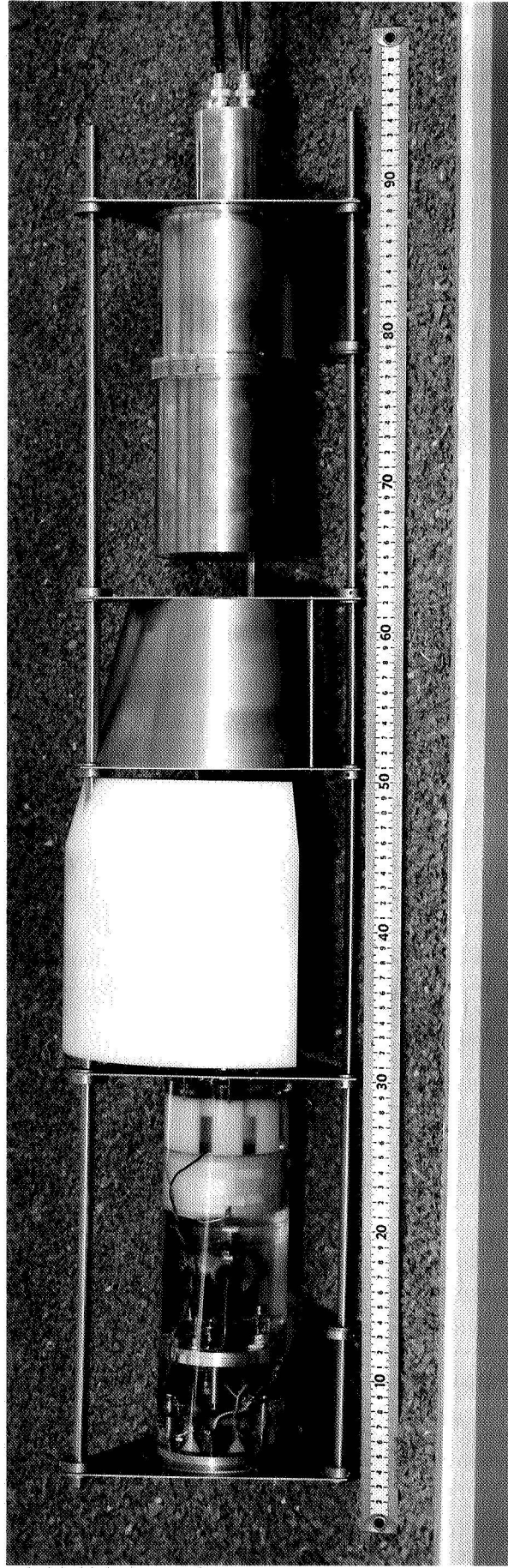


Figure No. 6-3

VIEW OF THE COMBINED-NEUTRON-EXPERIMENT DETECTOR PROBE (8 cm Polyethylene)

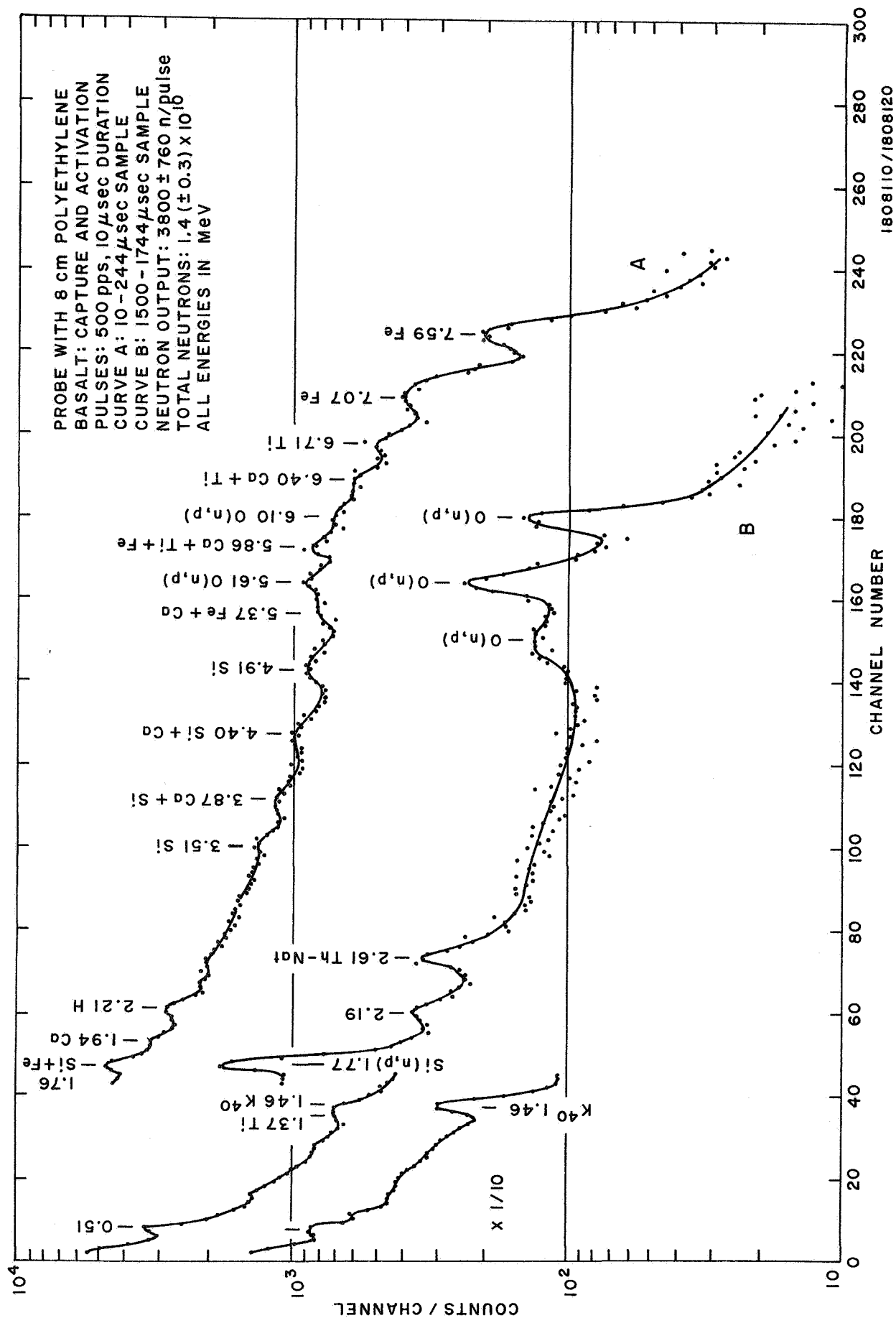


Figure No. 6-4

BASALT-CAPTURE AND CYCLIC ACTIVATION SPECTRA (Using Probe and 8 cm Polyethylene)

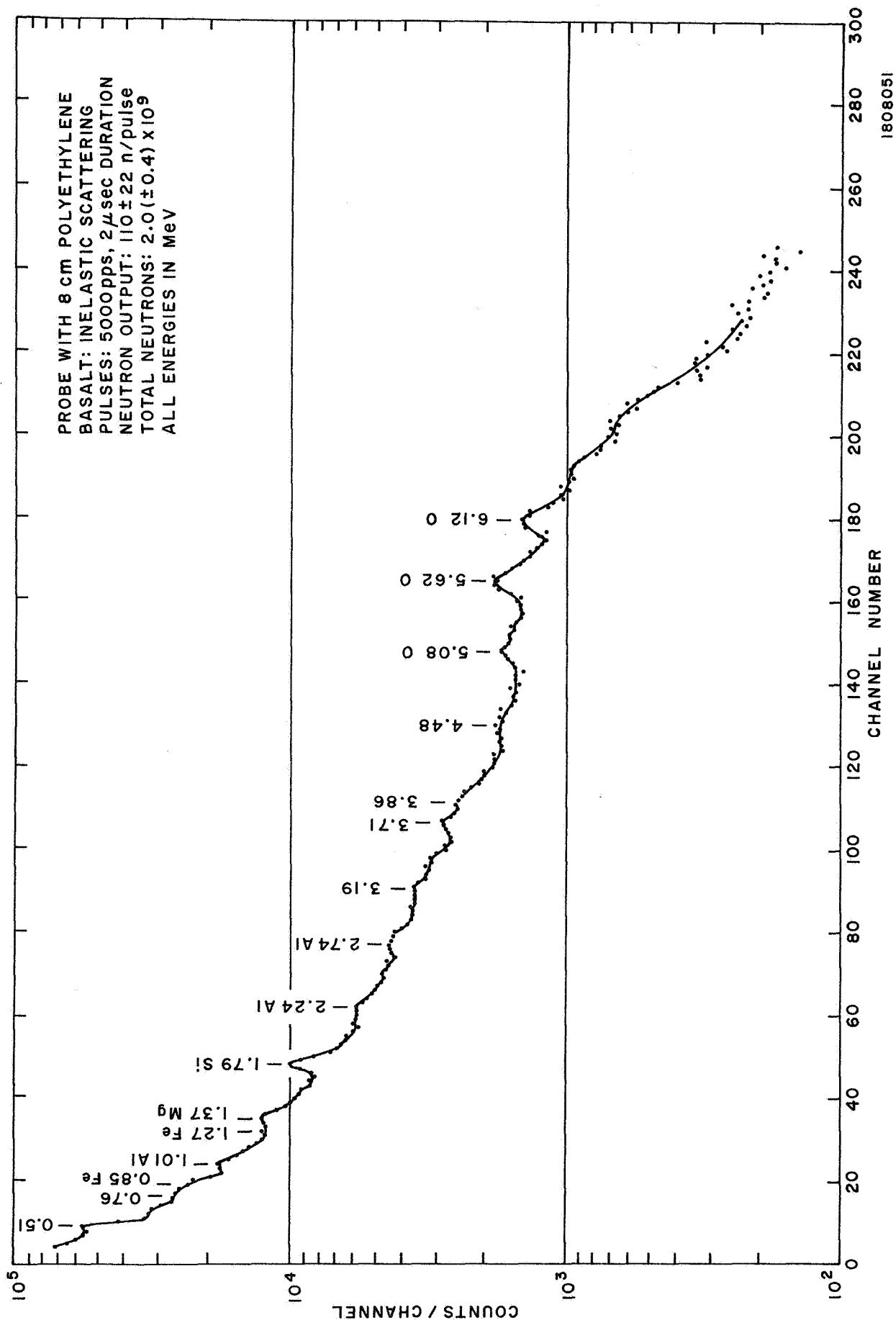


Figure No. 6-5

BASALT-INELASTIC SPECTRUM (Using Probe and 8 cm Polyethylene)